Non-coding RNA Research 12 (2025) 152–166

Contents lists available at ScienceDirect

Non-coding RNA Research

journal homepage: www.keaipublishing.com/en/journals/non-coding-rna-research

Original Research Article

Lnc-RAINY regulates genes involved in radiation susceptibility through DNA:DNA:RNA triplex-forming interactions and has tumor therapeutic potential in lung cancers

Emily S. Westemeier-Rice [a], Michael T. Winters [b], Travis W. Rawson [b], Kiran J. Patel [c], Olivia McHugh [b], Sierra Ward [b], Sarah McLaughlin [a], Amanda Stewart [a], Bishal Misra [d], Sebastian Dziadowicz [b], Weijun Yi [b], Sharan Bobbala [d], Gangqing Hu [b], Ivan Martinez [a,b,*]

[a] West Virginia University Cancer Institute, West Virginia University, West Virginia, United States
[b] Department of Microbiology, Immunology and Cell Biology, West Virginia University, West Virginia, United States
[c] West Virginia School of Medicine, West Virginia University, West Virginia, United States
[d] West Virginia University School of Pharmacy, West Virginia University, West Virginia, United States

ARTICLE INFO

Keywords:
lncRNA
NSCLC
Y chromosome
Senescence
Therapeutic nanoparticles

ABSTRACT

Lung cancer is the leading cause of cancer related deaths worldwide. Unfortunately, radiation resistance remains a major problem facing lung cancer patients. Recently, we identified a group of long non-coding RNAs (lncRNAs) known as linc-SPRY3 RNAs, expressed on the Y-chromosome, which play a role in radiation sensitivity by decreasing tumor burden *in vitro* and *in vivo* after radiation. In this study, we found that the linc-SPRY3 RNAs are one large lncRNA that we named *Ra*diation *In*duced *Y*-chromosome linked long non-coding RNA (lnc-RAINY). Through ATAC-seq and immunoprecipitation experiments, we show that lnc-RAINY interacts with DNA in a triple helix to induce chromatin remodeling and gene expression. We also identified that lnc-RAINY regulates CDC6 and CDC25A expression affecting senescence induction, cell migration patterns, and cell cycle regulation. Furthermore, the administration of Lnc-RAINY encapsulated in FDA-approved nanoparticles into a lung cancer patient-derived xenograft model dramatically reduces tumor progression demonstrating therapeutic potential.

1. Introduction

Lung cancer remains the leading cause of cancer-related deaths in the United States and worldwide [1]. Male patients have increased mortality rates of non-small cell lung cancer (NSCLC) [2]. While there have been many advances in the treatment of NSCLC, and the five year survival rate has increased to 23 %, from 15 % in the early 2000s, positive outcomes are few, thus research to identify new therapeutic targets to improve survival rates are ongoing [3]. One of the many treatments for NSCLC includes radiation therapy. However, there have been many proteins and pathways that have been implicated in resistance to radiation therapy, such as NOTCH [4], PI3K/AKT [5], UBE2T [6] and KRAS/mutantTP53 [7]. Further, males are less likely to respond to radiation therapy, when compared to females. This sex specific bias has been attributed to hormonal, genetic and environmental differences. As identified previously, part of this disparity may be in relation to the loss of Y chromosome in many cancers, including NSCLC. Therefore, novel therapies targeting radiation resistance imbued by these genes and the loss of Y chromosome are needed.

Recent studies have shown the importance of the noncoding genome in human diseases [8]. Of the many types of non-coding RNAs, long non-coding RNAs (lncRNAs) are some of the most versatile and multi-functional nucleic acids. Considered to be RNAs over 200 nucleotides and lacking major open reading frames, long noncoding RNAs have long been debated as to their number and importance, with some estimates ranging from just under 20,000 (ENCODE) to over 173,000 (NONCODEv6) in the human genome [9,10]. LncRNAs have been shown to bind and regulate chromatin [11,12], silence genes either directly or indirectly through modulation of microRNAs [13,14], and regulate post-transcriptional modifications [15,16].

Previously, we identified a group of lncRNAs named the linc-SPRY3 RNAs (linc-SPRY3-2, linc-SPRY3-3, and linc-SPRY3-4) originating from the Y chromosome [17]. This family has been identified to convey a radiation sensitive phenotype in NSCLC cell lines. We found that linc-SPRY3 RNAs interacted with the RNA binding protein IGF2BP3 and

* Corresponding author: Medical Center Drive, Rm 1818, Morgantown, WV, 26506, United States.
E-mail address: ivmartinez@hsc.wvu.edu (I. Martinez).

https://doi.org/10.1016/j.ncrna.2024.12.004
Received 27 August 2024; Received in revised form 1 December 2024; Accepted 7 December 2024
Available online 18 December 2024
2468-0540/. 2024 The Authors. Publishing services by Elsevier B.V. on behalf of KeAi Communications Co. Ltd. This is an open access article under the CC BY-NC-ND license (http://creativecommons.org/licenses/by-nc-nd/4.0/).

Abbreviations

lnc-RNAs long noncoding RNAs
lnc-RAINY Radiation induced Y chromosome linked long non-coding RNA
ATAC-Seq Assay for Transposase-Accessible chromatin with high-throughput sequencing
CDC6 Cell Division Cycle Protein 6
CDC25A Cell Division Cycle Protein 25A
NSCLC Non-Small Cell Lung Cancer
UBE2T Ubiquitin-Conjugating Enzyme E2T
IGF2BP3 Insulin Growth Factor 2 Binding Protein 3
HMGA2 High Mobility Group A2
RACE Rapid amplification of cDNA ends
AURKB Aurora Kinase B
RPI RNA-Protein Interaction Prediction
SetX Senataxin
POLDIP3 DNA Polymerase Delta Interacting Protein 3
UV-RIP Ultraviolet crosslinking and RNA Immunoprecipitation
UBC Ubiquitin Ligase C
lnc-HIF1a-AS1 Hypoxia Inducing Factor 1 alpha antisense 1 lncRNA
TTS Triplex Target Sites
DBD DNA Binding Domains
EPHA2 Ephrin Type-A Receptor 2
NR non-Radiated
IVT In vitro transcription
PDX Patient Derived Xenograft

consequently reduced the half-life of the antiapoptotic HMGA2 and oncogenic c-MYC mRNAs. To date, additional cellular functions by linc-SPRY3 RNAs have yet to be elucidated. In this study, we determined that the linc-SPRY3 RNAs are part of a larger lncRNA containing the 3 linc-SPRY3 RNAs termed *Ra*diation *In*duced *Y*-chromosome linked long non-coding RNA (lnc-RAINY). Additionally, we found that lnc-RAINY regulates several gene pathways involved in radiation sensitivity such as senescence, cell migration, and cell cycle progression by interacting with specific promoter regions in a triple helix conformation. Moreover, therapeutic administration of lnc-RAINY nanoparticles into a NSCLC patient -derived xenograft mouse model dramatically reduces tumor progression while simultaneously showing no toxicity *in vitro* and *in vivo*. Together, these findings show that lnc-RAINY is an important factor in male-specific response to radiation therapy.

2. Methods

2.1. ATAC-seq

Cells were prepared identically to RNA sequencing samples, in regard to siRNA knockdown and irradiation. After irradiation, 50,000 cells were removed for ATAC-Seq library preparation, the rest for further analysis to ensure effective knockdown of lnc-RAINY. The ATAC-Seq library was prepared as follows. Cells were centrifuged at 500×*g* at 4C for 5 min and supernatant was removed. Pellet was resuspended in RSB Buffer (10 mM Tris-HCl pH 7.4, 10 mM NaCl, 3 mM MgCl2, 1 μL/mL each of Digitonin, Tween 20 and NP40) and incubated on ice 3 min. RSB-without (10 mM Tris-HCl pH 7.4, 10 mM NaCl, 3 mM MgCl2, 1 μL/mL Tween 20) was added and the cells were centrifuged at 500×*g* for 10 min. Cells were resuspended in Transposition Mix (2x TD buffer 2.5 μL transposase (Illumina cat#20043196), 1 μL/100μL each of Digitonin and Tween 20, water and PBS). Tubes were then incubated at 37C shaking at 1000 rpm for 30 min. Reaction was cleaned using Qiagen PCR Purification Kit with 3M sodium acetate. Sample was eluted in an elution buffer and prepped for PCR Amplification. Barcoded Primers were added to each sample with 2x NEBNext Master mix (NEB cat#M0541S). Samples were PCR amplified for 12 cycles and purified using Qiagen PCR Purification Kit, eluted in water. Samples were loaded on a 2 % agarose e-gel and ran 3 min. Each lane was cut from the gel and the DNA extracted via Qiagen gel Purification kit. Samples were sent to the Genomics Core at West Virginia University for processing.

2.2. Cell culture

NSCLC cell lines H460, H820, H157, H1299, A549, and HEK-293T were cultured with DMEM (Gibco-Life Technologies, 12800-082). DMEM media was supplemented with 10 % FBS (Gemini Bio-Products, 100–106), l-glutamine (Gibco-Life Technologies, 25030-081), HEPES (GE Healthcare Life Sciences, SH30237.01), penicillin–streptomycin (Gibco, 15140-122), and amphotericin B (Gibco, 15290-026). All cells were grown in a humidified incubator at 37 °C in the presence of 5 % CO_2. Cell lines H460, H820, H157, A549, and H1299 were kindly provided by Dr. Erik A. Bey (Indiana University, Indianapolis, IN). Experiments conducted in these cell lines were performed within 2 weeks after thawing from liquid nitrogen (2–3 passages). All cell lines were tested for *Mycoplasma* and authenticated by ATCC using the *Mycoplasma* testing service and the Short Tandem Repeat profiling service.

2.3. Quantitative reverse transcriptase PCR

Total RNA was extracted using TRIzol Reagent (Ambion, 15596026) and chloroform as per manufacturer's instructions and then treated with Turbo DNAfree DNase (Invitrogen, AM1907) for 8 min at 37 °C. RNA concentrations were determined with a NanoDrop 2000 Spectrophotometer. 1 μg of total RNA was converted to cDNA using the iScript cDNA Synthesis Kit (Bio-Rad, 170–6891), followed by qRT-PCR using the SsoAdvanced Universal SYBR Green Supermix (Bio-Rad, 172–5271) and several pair of primers to specifically amplify the genes of interest in this study (Supplemental Table 1). Relative expression was calculated using the $\Delta\Delta C_t$ method [relative expression = 2-ΔC_t; where $\Delta C_t = C_t$ (Target RNA) – C_t (endogenous control RNA)], where the endogenous control for lncRNA and mRNA was GAPDH and/or UBC. PCR products were ran on a 1 % agarose gel with Ethidium Bromide at 100 V for 2 h. Gels were imaged on iBright imaging software.

2.4. UV crosslinked RNA immunoprecipitation

Cells were UV crosslinked and initially pelleted and frozen as described by Brownmiller et al. [17] Immunoprecipitations were then performed using a modified protocol from "RIP: An mRNA Localization Technique" - Jayaseelan et al., 2011 [18]. In brief, pellets were resuspended in 1x PLB (100 mM KCl, 5 mM $MgCl_2$, 10 mM HEPES at pH 7.00, 0.5 % Nonidet P-40 (Sigma I8896), 1 mM DTT, 200 Units/mL RNAse OUT (Invitrogen 10777-019) and one Complete Mini, EDTA-free Protease Inhibitor Tablet (Roche 11836170001))and frozen at −80 overnight. Dynabeads Protein G (Invitrogen 100-04D) were washed with NT-2 Buffer (NT-2 buffer: 150 mM Tris–HCl at pH 7.0, 100 mM Tris-HCl at pH 8.0, 750 mM NaCl, 5 mM MgCl2, and 0.25 % Nonidet P-40), and 5 μg antibody added (Rabbit IgG (Sigma N101-100UG) or Anti-Senataxin (Novus Bio NB100-57542)). Beads were rotated with the antibodies overnight, then washed 6 times with NT-2 Buffer, with the final resuspension in NET-2 Buffer (1 × NT-2 buffer supplemented with 20 mM EDTA at pH 8.0 (Ambion AM9260G), 1 mM DTT, 200 units/ml RNase OUT). Cell pellets were thawed and centrifuged, before supernatant was added to the designated tubes. Input was removed, before tumbling overnight at 4C. Beads were washed with 1x NT-2 Buffer six

times. Beads were resuspended in Proteinase K Buffer (1 × NT-2 buffer supplemented with 1 % sodium dodecyl sulfate (SDS) and 1.2 mg/mL Proteinase K (Ambion AM2546). The beads were then placed at 55C for 30 min before Phenol:Chloroform:Isoamyl Alcohol was added and the samples centrifuged for 10 min at 20,000×*g*. The supernatant was isolated and supplemented with 5M ammonium acetate, 7.5 M LiCl, 100 % Ethanol and left at −80C overnight. The isolated RNA was pelleted via centrifugation, washed with 80 % Ethanol. After centrifugation and removal of all ethanol, the pellets were resuspended in 20 μL RNAse free water (Ambion 9932). RNA was then used in further cDNA and PCR protocols, as described above.

2.5. S9.6 immunoprecipitation

Immunoprecipitations performed using a modified protocol from "Immunoprecipitation of DNA:RNA Hybrids using the S9.6 Antibody" - Gibbons and Aune 2020 [19]. Briefly, cells were fixed using formaldehyde and rotated for 10 min. Glycine was added for a further 5-min rotation, and the cells were pelleted and washed in PBS before pelleting again. The cells were then resuspended in hypotonic solution (20 mM Tris-HCl pH 7.4, 10 mM NaCl, 3 mM MgCl2) and incubated on ice for 15 min. 10 % NP-40 was added and the cells were pelleted after vortexing vigorously for 10s. The resulting pellet was then resuspended in R-loop digestion buffer (100 mM NaCl, 10 mM Tris pH8, 25 mM EDTA pH 8, 0.5 % SDS, 0.2 mg/mL Proteinase K) and left overnight at 65C. Phenol:Chloroform:Isoamyl Alcohol was added and mixed before spinning down at max speed. The top aqueous layer was collected and combined with 9M Sodium acetate and equivalent volumes of ice-cold isopropanol and 3 μg glycoblue (Invitrogen AM9516). The sample was incubated on ice for 10 min then pelleted at 21,000×*g* for 10 min at 4C before washing with 70 % Ethanol. Sample was resuspended in 500 μL FA Lysis buffer (CST 9803S) and sonicated using Diagenode Bioruptor (30 min on medium power, 30s on/30s off). 1.5 % agarose gel was used to validate sonication into ~500 bp fragments. 25 μL chromatin was reserved as input, 5–10 μg chromatin was used per antibody treatment. 5–10 μg sample was separated into 3 1.5 mL tubes before 10 μg antibody was added per designated tube (IgG (Calbiochem NI03-100μg), S9.6 (Sigma-Aldrich MABE 1095) x2), and the tubes were left to rotate overnight at 4C (12 h). Dynabead G per washed 4 times with TBST before being added to the tubes for a further 3-h rotation at 4C. All three tubes were given RNAse H buffer, but only one of the S9.6 antibody tubes received RNAse H (Thermo Scientific EN0201), and samples were incubated at 37 for 1 h before inactivation at 65C for 20 min. For the Promoter analysis specifically, RNAse H treatment was given before incubation with S9.6 IP antibody. Supernatant was removed for standardization and beads were washed with TBST 6 times, with 1 final wash in PBS, before resuspending beads in 20 μL water. ¼ sample was removed for DNA extraction, rest received DNAse I and DNAse I reaction buffer (NEB M0303S) and were incubated at 37 for 10 min before Trizol reagent was added. Samples were frozen at −80 overnight before undergoing 3 freeze/thaw cycles to help extract RNA from the beads. After the 3rd thaw, chloroform was added with vigorous vortexing. The sample was spun at max speed for 10 min at 4C, before the aqueous phase was transferred to a new tube, and isopropanol and glycoblue were added. RNA was spun, washed with 25 % ethanol and spun again at max speed for 10 min at 4C. All ethanol was removed before 10 min air dry. RNA was then resuspended in 21 μL water, and treated with TURBO DNAse (Invitrogen AM1907, 10 min at 37C, the 5 min incubation with DNAse inactivation reagent before pelleting inactivation reagent). RNA then proceeded to cDNA synthesis and qRT-PCR.

2.6. DNA extraction (trizol)

DNA was extracted according to manufacturer's instructions. Briefly, Trizol was added to Dynabeads G from S9.6 Immunoprecipitation reactions. Chloroform was added, and the samples were centrifuged at max speed for 10 min at 4C. The entire aqueous phase was removed, and 100 % Ethanol was added to the organic phases. The tube was inverted several times to mix and incubated at room temp for 3 min. The beads were then removed by a magnet, and the Trizol/ethanol was moved to a new tube. The tube was then spun for 7 min at 2000g at 4C to pellet the DNA. The pellet was then washed with 0.1M Sodium Citrate in 10 % Ethanol (pH 8.5) and sat for 30 min, with inversions every 10 min. After pelleting again at 200 g for 7 min at 4C, the supernatant was discarded, and the pellet was washed with 75 % Ethanol and incubated for 20 min before pelleting again. The pellet was then resuspended in 20 μL water and analyzed via qPCR.

2.7. siRNA transfection

Cells were transiently transfected with siRNAs according to Invitogen's Lipofectamine instructions. Per well of a 6 well plate, 9 μL Lipofectamine RNAiMax and 100 pmol siRNA were suspended in OptiMEM (Gibco Life Technologies, 31985-070) Sequences can be found in Supplementary Table 2. RNAiMax and siRNA were combined and rested for 5 min at room temperature. The mixture was added on top of plated cells dropwise. siRNA was given 12 h before radiation.

2.8. RNA sequencing

H460 and H820 cells were transiently transfected with siRNAs against linc-RAINY as described above. After the cells were re-attached, the plates were irradiated with 8gy radiation and left in standard growing conditions for 72 h. After collection, cells were RNA extracted as described above and RNA integrity was determined by an Agilent Bioanalyzer 2000 according to manufacturer instructions. Samples with a RIN >7 were sent to Admera for sequencing.

2.9. Lentiviral infection

Lentiviral particles were generated as previously described. (MD Anderson paper). Briefly, HEK-293T cells were transfected with lentiviral envelope plasmids (PsPax2, Addgene #12260 and VSV-G (Addgene #8454)) and either pLKO-shScramble (Addgene #1864) or two pLKO.1-TRC cloning vector (Addgene #10878) containing shRNA sequences against *linc-SPRY3-2 and linc-SPRY3-3* respectively), using Lipofectamine 2000. Media was changed after 12 h and the 293T cells were left for 24–48 h to generate virus. H460 and H820 cells were infected by filtering the viral particles through a 4 μm filter, supplementing with 1 μg/mL polybrene (Millipore Sigma, TR-1003-G) and adding directly to the target cells. Target cells were exposed for 24–48 h and allowed to recover for 48–72 h post infection. Cells were then stably selected via puromycin (1.0–2.5 μg/mL, Sigma Aldrich, P8833). Expression of target sequences was confirmed via qRT-PCR.

2.10. Retroviral transfection

Retroviral particles were generated as previously described. (MD Anderson). Briefly, HEK-293T cells were transfected with retroviral plasmid pBabe or pBabe containing the sequences of linc-RAINY (linc-SPRY3-Y, linc-SPRY3-2, linc-SPRY3-3, linc-SPRY3-4) or linc-RAINY and retroviral packaging plasmids (pclEco: Addgene #12371 and VSV-g: Addgene #8454) using Lipofectamine 2000. Media was changed after 12 h and the 293T cells were left for 48 h to generate virus. H1299 and A549 cells were infected by filtering the viral particles through a 4 μm filter, supplementing with 1 μg/mL polybrene (Millipore Sigma, TR-1003-G) and adding directly to the target cells. Target cells were exposed for 24–48 h and allowed to recover for 48–72 h post infection. Cells were then stably selected via puromycin (1.0–2.5 μg/mL, Sigma Aldrich, P8833). Expression of target sequences was confirmed via qRT-PCR.

2.11. Colony formation assay

Colony formation Assay was performed as previously described [17]. In brief, cells were treated with 8gy radiation, then seeded at a density of 25–250 cells per well of a 6-well plate (Falcon, 353046) After 14 days, plates were washed with 25 % PBS and stained with Crystal Violet in Methanol and left to dry overnight. Plates were then imaged using the Olympus MVX10 and quantified using ImageJ.

2.12. Annexin V Flow Cytometry

Cells were treated with 8gy radiation and collected 72 h after radiation. Cells were then collected and counted to reach 5 × 10^5 cells per sample. The cells were then pelleted and resuspended in Annexin V Binding Buffer (Invitrogen V13246). Annexin V FITC was added (Invitrogen A13199) and incubated for 10 min at room temperature in the dark. Binding buffer was added to the cells and the cells were pelleted. Additional binding buffer and Propidium Iodide was added. Samples then incubated for 5 min on ice before reading on the LSR Fortessa (RRID: SCR_017738).

2.13. Western blot

Cells were lysed in NP-40 lysis buffer (50 mM Tris-HCl pH 8.0, 150 mM NaCl, 1 mM EDTA, 1 % NP-40, 0.1 % SDS, 0.5 mM sodium metavanadate, Protease Inhibitor Cocktail (Sigma-Aldrich) for 12 min at 4 °C and clarified by centrifugation at 4 °C (5 min, 13,000 rpm). The concentration of extracted proteins was determined by using the Pierce BCA Protein Assay (Thermo Scientific, Rockford, IL). Cell lysates (30–50 μg of total cell protein) were separated by SDS-PAGE, transferred to Immobilon-Fl membranes (Millipore, Bedford, MA) and blocked with 5 % milk-TBST buffer (5 % nonfat dried milk, 25 mM Tris-HCl pH 8.0, 125 mM NaCl and 0.5 % Tween-20) for 1 h at room temperature. Membranes were incubated overnight at 4 °C with primary antibodies, washed with TBST and incubated with appropriate horseradish peroxidase (HPR)-conjugated secondary antibodies in 5 % milk- TBST buffer for 1 h at room temperature [1:10.000]. After rinsing with TBST, proteins were detected using the Pierce SuperSignal West Pico Chemiluminescent Substrate or Pierce SuperSignal West Femto Maximum Sensitivity Substrate (Thermo Scientific, Rockford, IL). The following primary antibodies were used: anti-Actin (mouse, Santa Cruz SC-47778), anti CDC6 (rabbit, Abcam 109315), anti-CDC25A (mouse, Invitrogen MA1-12293). The following secondary antibodies were used: anti-mouse IgG (CST 7076S) and anti-rabbit IgG (CST 7074S).

2.14. Cell cycle flow

Cells were treated with 8gy radiation and collected after 12 h. Samples were then fixed with 70 % Ethanol at 4C overnight. Samples were washed and resuspended in 0.2 % Tween 20 for 15 min at 37C. Samples were washed, RNAse A (180 μg/mL) and Propidium Iodide (Final Concentration 25 μg/mL) were added at room temperature. Samples were then covered and read on the Fortessa Flow Cytometer (LSR Fortessa: RRID: SCR_017738, S10 Equipment grant #OD016165) Data was analyzed using FCS Express.

2.15. Beta-galactosidase colorimetric assay

Cells were stained for the presence of Beta-galactosidase using Cell Signaling Technologies Kit #9860 as per manufacturer's instructions. In short, cells were seeded in 6 well plates and treated with 8gy Radiation. Cells were allowed to recover for 72 h prior to staining. Cells were washed with PBS. Cells were fixed with Fixative solution for 15 min at Room Temperature, then washed twice with PBS. beta-galactosidase solution was added and left overnight at 37C in an incubator without CO2. Cells were then imaged using an EVOS microscope. Beta-galactosidase positive cells were quantified using Cell Profiler.

2.16. Transwell migration assay

Treated cells were suspended in serum free media and seeded in the upper well of Costar Transwell Permeable Supports (Costar 3422, 8.0 μm polycarbonate membrane) plates at 1000–10,000 cells per well. Serum free media was added to the lower well of the plate. 10 % serum media was added to the lower chamber after 3 h. After 24 h, media was replaced in both chambers respectively. 24 h after media change, wells were washed with 25 % PBS and the remaining cells in the upper well were removed with a cotton swab. Cells on the bottom side of the transwell filter were fixed with 4 % formaldehyde in 25 % PBS for 5 min at R.T. Wells were washed and stained with 0.5 % Crystal Violet in 20 % Ethanol for 20 min at R.T. Stain was removed by 25 % PBS washes ×3 and the top of the well was cleaned once again with a cotton swab and left to dry overnight. Wells were imaged using the Olympus MVX microscope.

2.17. Generation of lnc-RAINY, GFP mRNA and FF-Luciferase mRNA

Each RNA sequence was cloned into pBABE vector containing a T7 promoter. In vitro transcription was performed using HiScribe T7 High Yield RNA synthesis Kit (NEB kit #E2040S) according to manufacturer's instructions. The RNAs were capped via G(5′)ppp(5″)G RNA cap structure analog Kit (NEB kit #S1407S) according to manufacturer's instructions. RNA was cleaned using the Monarch RNA Cleanup Kit (NEB kit #T2050S) according to manufacturer's instructions. RNA was quantified using Thermofisher Nanodrop 2000 before packaging.

2.18. Packaging RNA in nanoparticles

Materials- Cholesterol was obtained from Alfa Aesar (Haverhill, MA). DLin-MC3-DMA ionizable lipid was acquired from MedChemExpress (Monmouth Junction, NJ). All other lipid components used for LNPs were purchased from Cayman Chemical (Ann Arbor, MI, USA). Snake-Skin™ Dialysis Tubing (10 K MWCO) was obtained from Thermo Fisher Scientific Inc. (Waltham, MA, USA). Amicon ® Ultra Centrifugal Filter, 30 kDa MWCO was obtained from Sigma-Aldrich (St. Louis, MO). QuantiFluor® RNA System was obtained from Promega Corporation (Madison, WI). Fluorescence was read using SpectraMax iD5 microplate reader. *Formulation and characterization of lipid nanoparticles*– Lipid nanoparticles (LNPs) were formulated using the flash nanoprecipitation (FNP) method with the help of a Confined Impinging jet (CIJ) mixer, as previously described [20]. DMG-PEG 2000, 1,2-Distearoyl-sn-glycero-3-PC (1,2-DSPC), cholesterol, and DLin-MC3-DMA were used in 1.5: 10: 38.5: 50 percent molar ratio. All the lipids were dissolved in ethanol and the mRNA was dissolved in 50 mM sodium citrate buffer (pH 4). The organic and aqueous phases impinged together in the CIJ mixer to form LNPs, collected in a 2 mL reservoir containing 50 mM (sodium citrate, pH 4). The organic solvent from the formulations was removed through dialysis using phosphate-buffered saline (PBS) and a 10 kDa dialysis membrane for 3 h. Diluted LNP formulations were concentrated using the Amicon ® Ultra Centrifugal Filter, 30 kDa MWCO. The particle size of lipid nanoparticles (LNPs) was evaluated using Dynamic Light Scattering (DLS) from Malvern Instruments (UK). PBS was utilized for all measurements. The encapsulation efficiency of RNA in LNPs was measured using the QuantiFluor® RNA System. LNPs were monodisperse, with sizes ranging between 120 and 140 nm. The encapsulation efficiency of the RNA inside the LNPs was greater than 90 %.

2.19. Tumor growth assay

PDX WVU-Ma-0009, generously provided by Dr. Patrick Ma (Penn State), and housed under the Genetic Tumor Models Core facility at West Virginia University, was dissociated using Miltenyi's tumor dissociation

kit according to manufacturer's instructions (Miltenyi Biotec, Cat. 130-095-929), resuspended in 5 % Matrigel, and injected subcutaneously into the right flank of male mice. Alternatively, H1299 cells were trypsinized and suspended at 5×10^6 cells/mL in Matrigel. A total of 1×10^6 cells were injected subcutaneously into the right flanks of male NSG mice (NOD.Cg-Prkdc^{scid} Il2^{rgtm1Wjl}/SzJ (NSG) immunodeficient mice, bred inhouse at WVU under the Genetic and Tumor Model Core). Mice were housed in the West Virginia University Animal Facility under pathogen-free conditions with the approved Institutional Animal Care and Used Committee (IACUC) protocol number: 2309070219. All animal experiments comply with National Institutes of Health guide for the care and use of Laboratory animals (NIH Publications No. 8023, revised 1978). Once tumors reached ±75 mm^3, nanoparticles were given as a bolus dose, delivered intratumorally, at a dose of 72.1 μg Nanoparticles per 100 mm^3 of tumor. 24 h post injection, radiotherapy was started, with a second bolus injection immediately following radiation on day 2. A total of 4 treatment groups (3 animals each) included *sham-treated control* (0 Gy): receiving GFP/Luciferase mRNA loaded nanoparticles or lnc-RAINY loaded nanoparticles, and *radiation* (20 Gy, 4 fractions): receiving GFP/Luciferase mRNA loaded nanoparticles or lnc-RAINY loaded nanoparticles. Tumor volume and depth was measured using ultrasound imaging (Vevo F2, FUJIFILM VisualSonics Inc.). Measurements were quantified using the Vevo LAB 2.2.0 software. Tumors were assessed until they reached >1000 mm^3, day 17 after initiation of treatment, or mice showed evidence of morbidity. Relative tumor volume was determined by normalizing measured volumes to the starting volume (day 0) of each respective animal.

2.20. Statistical analysis

Are presented as mean ± SD (*, $P < 0.05$; **, $P < 0.01$; ***, $P < 0.001$). The statistical significance between experimental groups was determined by students T test, unless comparing 4 groups, samples were analyzed with two-way ANOVA followed by Tukey multiple comparisons test. Analyses were performed using GraphPad Prism V8 and Microsoft Excel 2013.

3. Results

3.1. The linc-SPRY3 RNAs are part of a larger lncRNA expressed from the Y chromosome

By using a lncRNA microarray for global gene expression analysis, our previous study in 2020 by Brownmiller et al. showed that the linc-SPRY3 RNAs (linc-SPRY3-2, linc-SPRY3-3, and linc-SPRY3-4) were differentially overexpressed after radiation treatment in male NSCLC cell lines [17]. These linc-SPRY3 RNAs are expressed from the DYZ1 region on the Yq12 arm of the Y chromosome, a highly repetitive region of DNA tandem repeats just recently fully sequenced in 2023 [21]. Surprisingly, Brownmiller et al. found that utilizing shRNA designed specifically against linc-SPRY3-2 or linc-SPRY3-3 repressed all three linc-SPRY3 RNAs. Furthermore, virtual northern blots identified an overlapping peak over 3000 nt using all 3 linc-SPRY3 RNAs primer sets, even though the LNCipedia database predicts their sizes between 204 and 776 nt, suggesting that these lncRNAs were part of a much longer lncRNA [17,22]. In 2006, a previous publication by Jehan et al. identified and cloned two long RNAs originating from the Yq12 DYZ1 region in testis named AK47 (AK128024.1 + AY598347.3) and AY598346.2 [23]. Interestingly, not only were we able to find the sequences of all 3 linc-SPRY3 RNAs been part of these two cDNAs (Supplementary Figure 1A), but also because of the recently fully sequenced DYZ1 region, we were able to identify an overlap between these two RNAs sequences near the 5′ end of AK47 and the 3′ end of AY598346.2 (**Supplementary Figure 1A**). In order to verify the existence of this long lncRNA, we designed overlapping primers covering the entire transcript (Supplementary Figure 1A, Supplementary Table 3) for RT-PCR amplification and sequencing using testis RNA and NSCLC H460 cell line. We accurately amplified the predicted sizes of this lncRNA from nucleotide 595 to 3050 using several primer combinations (Supplementary Figure 1B and C) including the AK-47 and AY598346.2 overlapping region (primers covering nucleotides 949 to 1454). Sequencing of all amplified regions were performed confirming the specificity of amplification including the overlapping region (Supplementary Figure 1D). After confirming the existence of this larger lncRNA we named it Radiation Induced Y-chromosome linked long non-coding RNA (lnc-RAINY). Due to the highly repetitive nature of this lncRNA, we were unable to directly amplify the full length utilizing the previously designed primers. Therefore, we used Gibson assembly cloning to clone the full length lnc-RAINY into a pBABE retroviral expression vector (Supplementary Fig 1E) as well as 3 different fragments of lnc-RAINY each one containing one of the linc-SPRY3 RNAs (5′ fragment contains linc-SPRY3-3, middle fragment contains linc-SPRY3-2, and 3' fragment contains linc-SPRY3-4) (Supplementary Fig 1F). Exogenous expression of lnc-RAINY was confirmed in NSCLC cell line H1299 by using the 3 sets of primers developed to amplify the linc-SPRY3 RNAs (Supplementary Fig 1G). Furthermore, full length lnc-RAINY as well as lnc-RAINY fragments increased radiation sensitivity when overexpressed in H1299 cells (Supplementary Figure 1H), suggesting that all regions in this transcript are involved in inducing radiation sensitivity.

3.2. The repression of lnc-RAINY affects the expression of genes involved in cell cycle regulation, senescence, and migration

To identify alterations in gene expression due to the repression of lnc-RAINY in NSCLC cell lines with or without radiation treatment, RNA sequencing was performed in two Y-chromosome positive NSCLC cell lines H460 and H820. Specifically, a combination of siRNAs targeting the three distinct linc-SPRY3 RNA sequences within lnc-RAINY and combined as siPool (siRNA Lnc-RAINY) were designed; the resulting gene expression was compared to control siRNA (siRNA CTRL) and each individual siRNA, with or without single dose, 8gy radiation treatment. Differentially expressed genes (fold change 1.5), varied between each treatment type, however there were 38 genes identified to be differentially expressed at the convergence of all treatment modalities (Fig. 1A and B). Gene ontology enrichment analysis of differential expression identified changes related to DNA replication, cell cycle regulation, and cell migration upon loss of lnc-RAINY. (Fig. 1C). Validation of the differentially expressed genes via qRT-PCR showed in H460 and H820 NSCLC cell lines, loss of lnc-RAINY activity increased expression of critical cell cycle genes CDC6 and CDC25A, drug resistance, and migration gene AURKB and decreased expression of inflammatory response gene S100A9. (Fig. 1D and Supplementary Figure 2A). This was further validated at the protein level for CDC6 and CDC25A (Fig. 1E). Important in cell cycle regulation, experimental evidence suggests that CDC6 and CDC25A are involved in migration (CDC6) [24,25] and senescence (CDC25A) [26–28] in NSCLC carcinogenesis. Radiation has been shown to induce both migration and senescence, with both mechanisms used as methods to resist radiation therapy [29,30]. Overall Survival is decreased in patients with overexpression of CDC6 and CDC25A (Fig. 1F). Overexpression of lnc-RAINY in the H1299 NSCLC cell line, which lack lnc-RAINY expression as a result of loss of Y chromosome, downregulated of CDC6 and CDC25A (Supplementary Figure 2B). Interestingly, upon breaking down lnc-RAINY into three fragments containing the linc-SPRY3 RNAs previously identified, we were not able to see downregulation of CDC6 or CDC25A expression suggesting that the presence of the entire lnc-RAINY transcript is necessary for the regulation of these genes (Supplementary Figure 2C). Together, these results indicate that lnc-RAINY alters gene expression, particularly of genes involved in cell cycle, senescence, and migration.

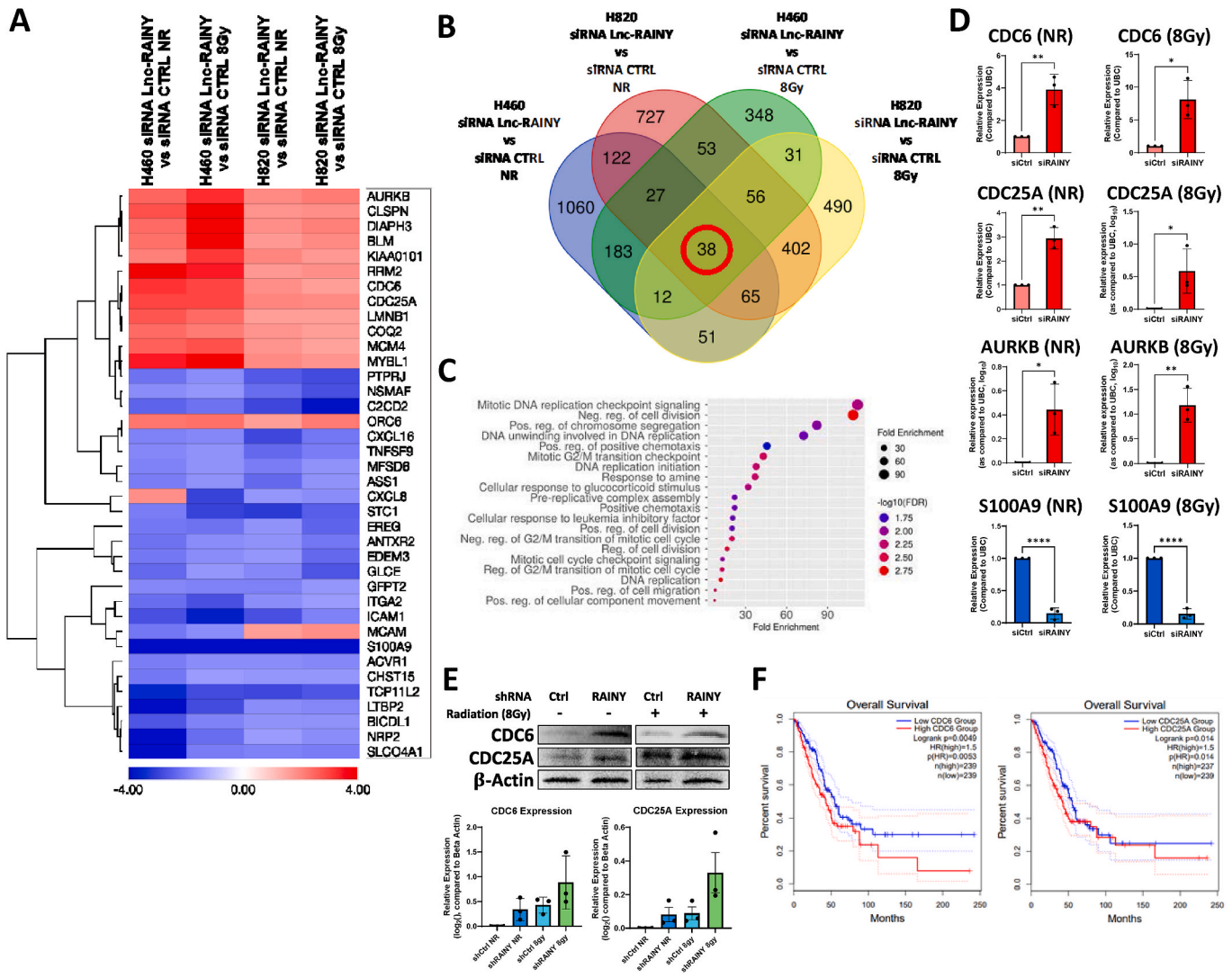

Fig. 1. Lnc-RAINY knockdown alters gene expression of cell cycle regulation, senescence, and migration.
A. Venn diagram of differentially expressed genes showing 38 genes identified as differentially expressed regardless of radiation status and lnc-RAINY presence. **B**. Heatmap of the 38 differentially expressed genes aligned with cell lines H460 and H820. **C**. Pathway analysis of differential genes showed the greatest effect on Mitotic DNA replication checkpoint signaling and the negative regulation of cell division upon loss of lnc-SPRY3 RNAs. **D**. qRT-PCR validation of RNA-Sequencing results, showing increased expression of CDC6, CDC25A, RRM2 and Aurora Kinase B genes in non-radiated (NR) and radiated (8Gy) H460 cells. **E.** Immunoblotting validation of RNA-sequencing results showing higher CDC6 and CDC25A protein expression in non-radiated and radiated H460 cells with lnc-RAINY knockdown. **F.** Kaplan Meier Curves showing increased expression of CDC6 and CDC25A are associated with decreased overall survival in Lung Adenocarcinoma. Curves generated by Gepia2. Data are presented as mean ± SD (*, $P < 0.05$; **, $P < 0.01$; ***, $P < 0.001$). The statistical significance between experimental groups was determined by students T test.

3.3. The lnc-RAINY forms DNA:DNA:RNA triplex and regulates CDC6 and CDC25A by interacting with their promoters at the chromatin level

Our previous work has shown that lnc-RAINY expression increases after radiation treatment and is localized exclusively in the nucleus [17]. Additionally, we have also shown that lnc-RAINY interacts with RNA binding proteins such as IGF2BP3 [17]. We therefore hypothesized that lnc-RAINY may be interacting either directly with the DNA or by recruiting RNA binding proteins to help modify the expression of genes such as CDC6 and CDC25A. Thus, the Assay for Transposase-Accessible chromatin with high-throughput sequencing (ATAC-Seq) was used to determine changes in chromatin remodeling due to lnc-RAINY-chromatin interaction. We identified 217 ATAC-seq peaks increased, representing open chromatin regions mostly mapped near transcription start sites, and 977 ATAC-seq peaks decreased after knockdown of lnc-RAINY in H820 cells (Fig. 2A). Interestingly, we specifically identified increase of ATAC-seq peaks at the promoter regions of CDC6, CDC25A and AURKB, correlating with higher expression of these genes after lnc-RAINY knockdown in H820 cells (Fig. 2B). Additional analysis of the sequence of lnc-RAINY led us to hypothesize it may be recruiting chromatin modifiers. Performing RNA-Protein Interaction Prediction (RPI) [31] identified two RNA-protein interactions of interest: Senataxin (SETX), a DNA:RNA Helicase, generally known to interact with DNA:RNA hybrids or R-loops, particularly at DNA Double Stranded breaks [32] and DNA Polymerase Delta Interacting Protein 3 (POLDIP3), shown to disrupt the formation for DNA:RNA hybrids [33]. In this analysis, both SETX and POLDIP3 had a greater predicted interaction score as compared to previously published data from IGF2BP3 (Fig. 2C). To validate these findings, UV crosslinking and RNA immunoprecipitation (UV-RIP) was performed using an antibody against SETX protein in H460 cells and were able to specifically pulldown lnc-RAINY and not the negative control UBC mRNA (Fig. 2D). Because SETX is a helicase, known for its R-loop interactions, we hypothesized that lnc-RAINY interacts with DNA in a triple helix, or R-loop. To test

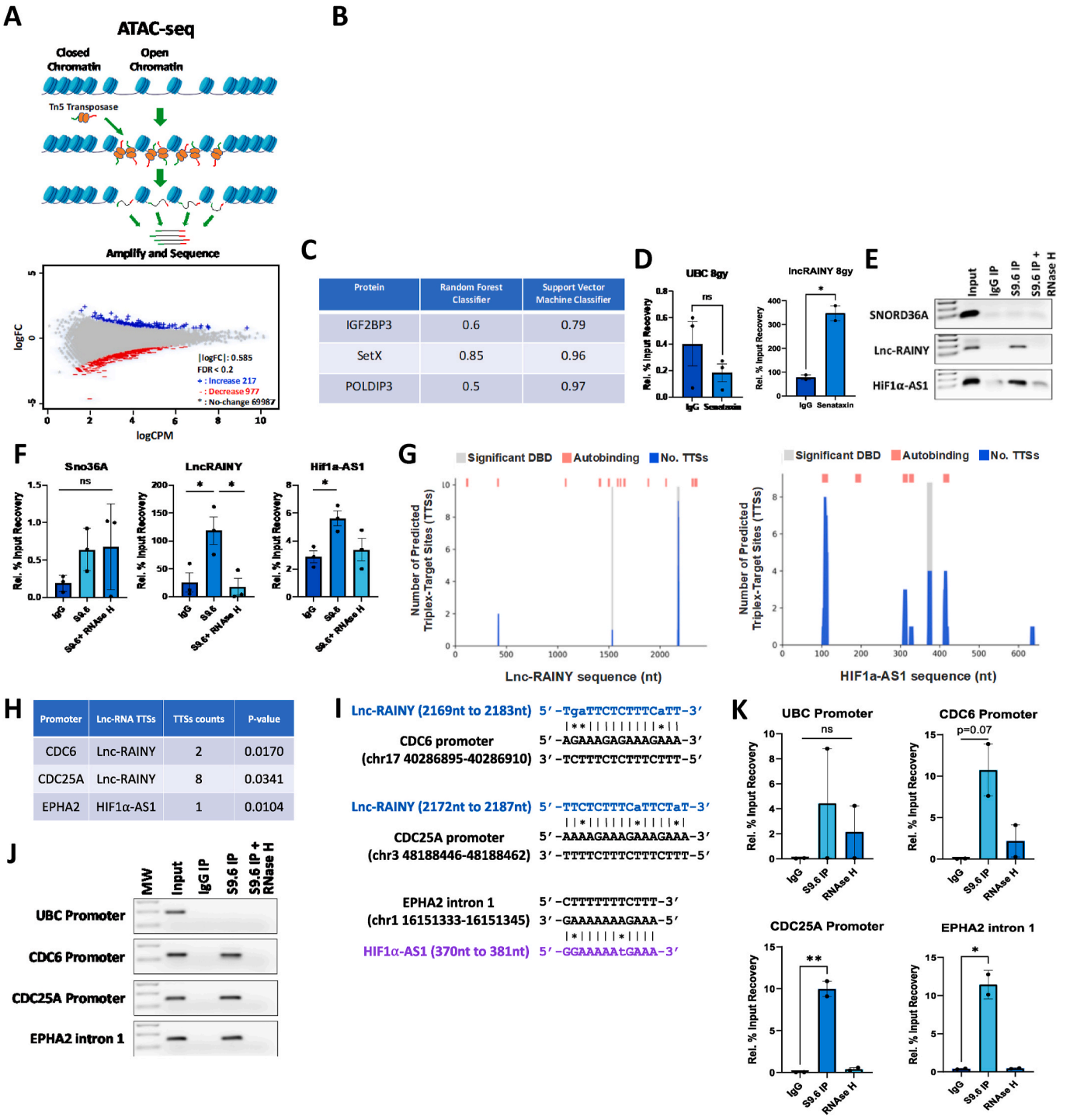

Fig. 2. Lnc-RAINY interacts with DNA in a triple helix to help control chromatin accessibility.
A. Model of ATAC-Seq and Volcano plot showing differentially accessible chromatin sites (FDR <0.2, p < 0.05). **B.** Open promoter regions (Blue arrows) of CDC6, CDC25A and AURKB after lnc-RAINY knockdown via siRNA. **C.** Predictive models computed by RPI-Seq (Iowa State) of RNA-Protein interactions identified SetX and POLDIP 3 as likely candidates for lnc-RAINY interactions. **D.** UV Crosslinking and RNA immunoprecipitation identified interaction of lnc-RAINY with Senataxin (SETX) protein. **E-F.** S9.6 Immunoprecipitations recovered lnc-RAINY and HIF1a-AS1 as part of DNA:DNA:RNA triplex-forming interactions. **G**. Output from a predictive triplex-target site software (rgt-TDF) identifying lnc-RAINY binding sites to CDC6 and CDC25A Promoter at length 16 base pairs, and positive control HIF1a-AS1 had binding to the EPHA2 promoter at 12 base pairs. **H.** Chart output of rgt-TDF with triplex domain sites and p-values. **I.** Identification of specific base pairs between lnc-RAINY and CDC6 and CDC25A promoter regions identified by rgt-TDF. **J-K.** Amplification of promoter regions from genes UBC, CDC6, CDC25A and EPHA2 after immunoprecipitation with S9.6 antibody. Data are presented as mean ± SD (*, $P < 0.05$; **, $P < 0.01$; ***, $P < 0.001$). The statistical significance between experimental groups was determined by students T test.

this, we used the S9.6 antibody that recognizes DNA:DNA:RNA triplexes and performed RNA Immunoprecipitation (RIP) assays. Notably, we were able to recover lnc-RAINY using the S9.6 antibody in H460 cells, as well as lnc-RNA HIF1a-AS1, previously shown to form DNA:DNA:RNA triplex-forming interactions [34], and not our negative control SNORD36A (Fig. 2E and F). The recovery of lnc-RAINY and HIF1a-AS1 was lost after exposing the samples to RNase H, a ribonuclease that degrades RNA when is interacting with DNA (Fig. 2E and F), highlighting the DNA:DNA:RNA triplex-forming interactions of these lncRNAs. Furthermore, we used a triplex-target sites (TTSs) predictor software [35] and found 3 TTSs regions in Lnc-RAINY with two of them having significant DNA binding domains (DBD), as well as 6 TTSs regions in HIF1a-AS1 with one of them having significant DBD (Fig. 2G). Then, we analyzed the promoter regions of CDC6 and CDC25A for potential TTSs with lnc-RAINY and found two TTSs sites in CDC6 and 8 TTSs sites in CDC25A (Fig. 2H and I). We also found a TTSs site in the intron 1 region of EPHA2 that has been shown previously to interact with HIF1a-AS1(Fig. 2H and I). Having identified these TTSs sites, analyzed the DNA recovered from the S9.6 IP and we were able to detect the promoter regions for CDC6 and CDC25A, as well as the EPHA2 intron region but not the UBC promoter region (Fig. 2J and K). Taken together, these results indicate lnc-RAINY regulates specific genes

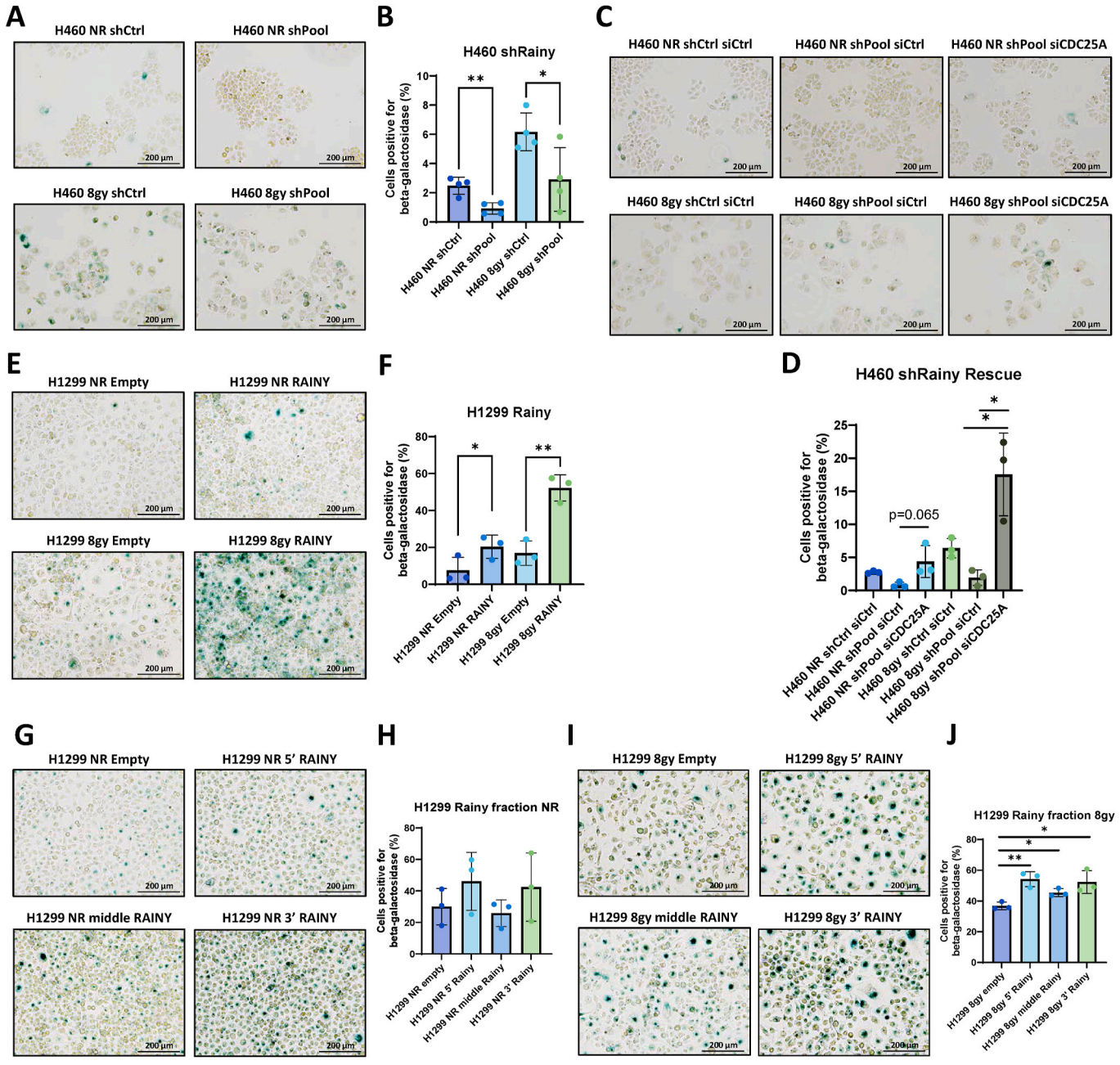

Fig. 3. Lnc-RAINY interacts with CDC25A to impact senescence.
A-B. Beta-galactosidase staining of H460 cells with (8gy) and without (NR) radiation, showing a decrease in senescent cells after knockdown of lnc-RAINY (shPool). **C-D.** Knockdown of CDC25A significantly increased the percentage of senescent cells after radiation. **E-F.** Beta-galactosidase staining of H1299 cells with and without radiation, showing an increase in senescent cells after overexpression of lnc-RAINY. **G-H.** Beta-galactosidase staining of H1299 cells without radiation. **I-J.** Beta-galactosidase staining of H1299 cells with the fragments of lnc-RAINY after radiation, showing an increase in senescent cells after overexpression of lnc-RAINY fragments. Data are presented as mean ± SD (*, $P < 0.05$; **, $P < 0.01$; ***, $P < 0.001$). The statistical significance between experimental groups was determined by students T test.

through DNA:DNA:RNA triplex-forming interactions.

3.4. Lnc-RAINY modulates senescence through CDC25A

CDC25A has been shown to play a role in senescence, with its expression significantly decreased during the process of irreversible growth arrest [26]. Therefore, a beta-galactosidase staining assay was utilized to identify senescent cells after the repression of lnc-RAINY in non-radiated (NR) or 8Gy radiated (8Gy) H460 and Y-chromosome positive H157 NSCLC cell lines. Absence of lnc-RAINY decreases the number of senescent cells with and without radiation (Fig. 3A and B and Supplementary Figure 3A). Furthermore, by knocking down CDC25A via siRNAs in lnc-RAINY positive cell lines with shRNA against lnc-RAINY, we saw an increase in senescent cells after radiation, suggesting that CDC25A is partially responsible for the repression of a senescent phenotype after the reduction of lnc-RAINY expression (Fig. 3C and D). On the other hand, exogenous expression of lnc-RAINY in H1299 and Y-chromosome negative A549 NSCLC cell lines increased the number of senescent cells regardless of radiation exposure (Fig. 3E and F and Supplementary Figure 3B). Additionally, H1299 cells with individual lnc-RAINY fragments showed increased senescence after radiation and no changes without radiation (Fig. 3G–J). Overall, these data suggest that lnc-RAINY increases senescence after radiation, in part through the modulation of CDC25A expression.

3.5. Lnc-RAINY alters migration through CDC6

Increased expression of CDC6 has been shown to increase the migratory ability of tumor cells [25]. Because lnc-RAINY knockdown increases expression of CDC6, we examined the migratory ability of H460 cells with and without lnc-RAINY. By using transwell migration assays, we found that knocking down lnc-RAINY increases the migratory ability of H460 cells without radiation (Fig. 4A and B). To verify if this interaction was likely through CDC6 expression, we performed a siRNA mediated knockdown of CDC6 in lnc-RAINY positive cell lines with siRNA against lnc-RAINY. There was a marked decrease in migration, with a near complete return to migration levels in H460 cells after knocking down CDC6 and lnc-RAINY, suggesting that CDC6 is partially responsible for the migration phenotype induced by lnc-RAINY (Fig. 4C and D). Conversely, exogenous expression of lnc-RAINY in H1299 and A549 cells decreased their ability to migrate after radiation treatment. (Fig. 4E and F and Supplementary Figure 4A). Further analysis showed that the fragments of lnc-RAINY showed a differential change in migratory ability, with the central fragment of lnc-RAINY having the greatest impact on migration (Fig. 4G and H). These data suggest that lnc-RAINY impacts migration by decreasing expression of CDC6.

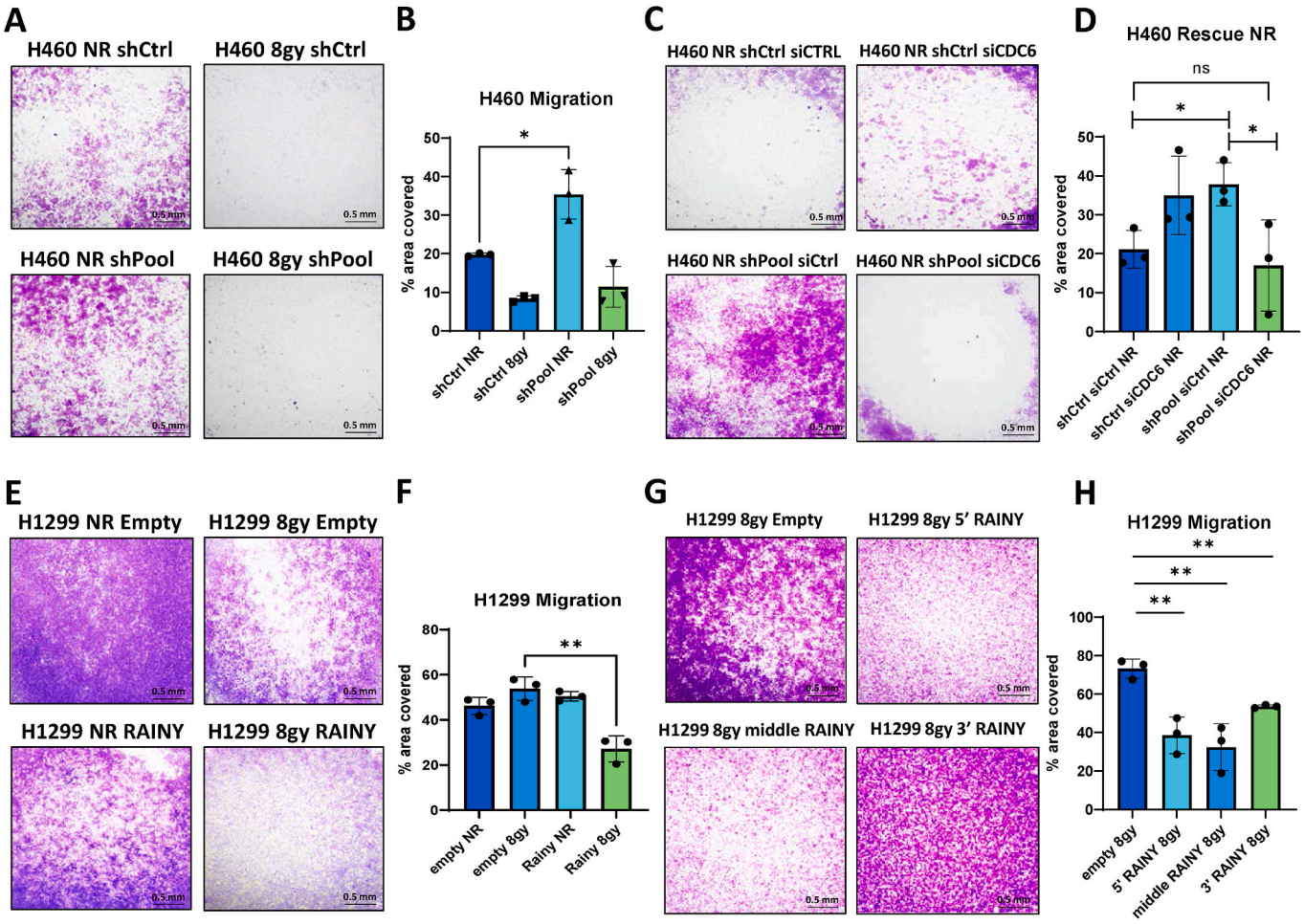

Fig. 4. Lnc-RAINY interacts with CDC6 to impact migration.
A-B. Transwell migration assays show increase in cell migration in non-radiated H460 cells with knockdown of lnc-RAINY (ShPool). **C-D.** Transwell migration assays show a rescue phenotype in non-radiated H460 cells after knockdown of lnc-RAINY (ShPool) and CDC6 (siCDC6). **E-F.** Transwell migration assays show decrease in cell migration in radiated (8gy) H1299 cells exogenously expressing lnc-RAINY. **G-H.** Transwell migration assays show decrease in cell migration in radiated (8gy) H1299 cells exogenously expressing the fragments of lnc-RAINY. Data are presented as mean ± SD (*, $P < 0.05$; **, $P < 0.01$; ***, $P < 0.001$). The statistical significance between experimental groups was determined by students T test.

3.6. Lnc-RAINY expression impacts cell cycle progression and cell proliferation

Radiation resistance is an important issue facing patients diagnosed with NSCLC [36]. As both CDC6 and CDC25A are cell division cycle proteins, we hypothesized lnc-RAINY would impact the ability of cells to progress through the cell cycle after DNA damage, as cells are the most radio sensitive in the G2 and M phases of the cell cycle [37]. Flow cytometry showed that radiated H460 cells were paused in G1 phase and reduced in G2 phase when lnc-RAINY was knocked down (Fig. 5A and B). On the other hand, exogenous expression of lnc-RAINY in H1299 cells pause the cells in G2 phase and reduced the number of cells in S phase in non-radiated cells (Fig. 5C and D). The changes in the Y-chromosome positive H460 cells after radiation were likely due to lnc-RAINY base expression levels, which is very low before radiation but increase significantly after radiation. Conversely, the changes in the Y-chromosome negative H1299 cells exogenously expressing lnc-RAINY being significantly different without radiation but not in radiated H1299 cells may indicate some level of gene expression background noise caused by the radiation treatment. Breaking lnc-RAINY down into its three fractions did not show any difference in cell cycle progression, regardless of radiation status, indicating the cell cycle regulation was likely through the full-length lnc-RAINY transcript (**Supplemental Figure 5A and B**). Interestingly, exogenous expression of lnc-RAINY full-length or the three fractions caused a minor decrease in proliferation in non-radiated H1299 cells (**Supplemental Figure 5C**). CDC6 and CDC25A knockdown in cells with siRNA against lnc-RAINY did not recover cell cycle phases suggesting that lnc-RAINY regulates cell cycle through other genes (**Supplemental Figure 5D and E**). Overall, these data suggest that lnc-RAINY changes the ability of cells to progress through the cell cycle and may decrease proliferation after radiation.

3.7. Lnc-RAINY can be delivered via nanoparticles to induce radiation sensitivity in vitro and in vivo

Our data shows that lnc-RAINY plays an important role in the regulation of cellular pathways involved in radiation susceptibility, suggesting that lnc-RAINY could be used as a radio-sensitizing agent, if given to NSCLC tumors before radiation treatment. Therefore, we *in vitro* transcribed (IVT) lnc-RAINY and packaged the lncRNA in DLin-MC3-DMA nanoparticles as a method for delivery. To validate the expression of lnc-RAINY after nanoparticle treatment, we measured lnc-RAINY expression in H1299 and H460 cells and confirmed expression of lnc-RAINY (Supplemental Figure 6A and B). We further validated the potential toxicity of exogenously delivered lnc-RAINY by measuring levels of cellular senescence. Specifically, we show lnc-RAINY has no impact on the levels of cellular senescence of immortalized normal male lung epithelial cell line NuLi-1 and a minor impact on immortalized normal female lung epithelial cell line HBEC-3KT (Fig. 6A and B), suggesting very low toxicity in normal cells. Next, we treated H1299 and A549 cells with lnc-RAINY nanoparticles and saw an increase in senescence after radiation, as expected. (Fig. 6C and D). To further test these nanoparticles *in vivo*, we injected H1299 NSCLC cells into the flanks of male mice. When tumors reached 75 mm^3 we treated them intratumorally with 2 doses of lnc-RAINY or GFP mRNA loaded nanoparticles at 72.1 μg Nanoparticles per 100 mm^3 of tumor on days 0 and 2 and treated with 4 doses of 5 Gy radiation across days 1–4. (Fig. 6E). The presence of lnc-RAINY significantly decreased tumor burden after radiation and decreased tumor growth rates (Fig. 6F and G and Supplemental Figure 6C). To further test this with a more heterogenous tumor model, we treated a NSCLC patient derived xenograft (PDX) tumor obtained recently in our clinic (WVU-Ma-0009) with the same condition previously described for H1299 cells. We saw a dramatic decrease in tumor size, burden and growth rate regardless of radiation status (Fig. 6H–J). Because lnc-RAINY is derived from the Y chromosome, we focused exclusively on the treatment of male PDXs within male mice. Further

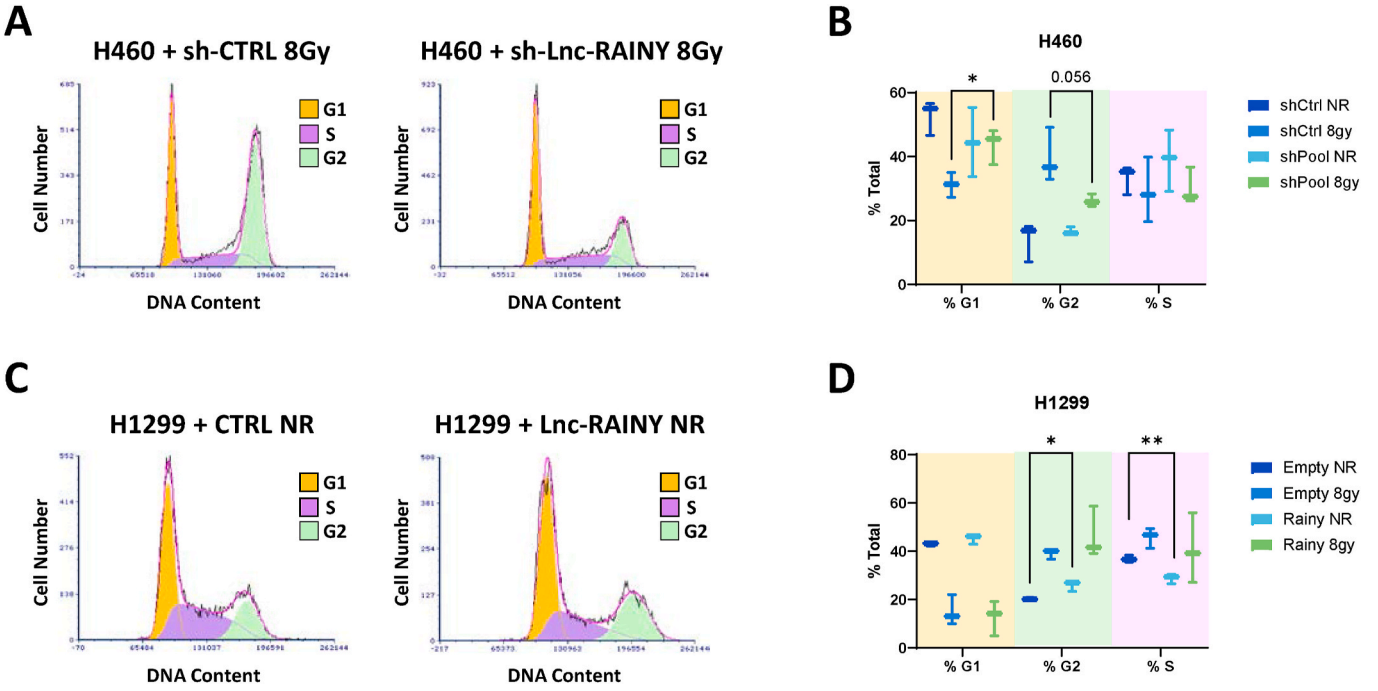

Fig. 5. Lnc-RAINY impacts cell cycle progression
A. Flow cytometry of cell cycle showing an increase in G1 phase and a decrease in G2 phase in H460 cells after lnc-RAINY knockdown and radiation treatment (8gy). **B.** Box plot quantification of (A). **C.** Flow cytometry of cell cycle showing an increase in G2 and decrease in S phase in non-radiated H1299 cells after lnc-RAINY exogenous expression. **D.** Box plot quantification of (C). Data are presented as mean ± SD (*, $P < 0.05$; **, $P < 0.01$; ***, $P < 0.001$). The statistical significance between experimental groups was determined by students T test.

data is needed to test the effectiveness of lnc-RAINY in female PDXs, in female mice. These compelling data suggest that lnc-RAINY can be further studied as a treatment to increase the radiation sensitivity of NSCLC tumors. In particular, clinically, this treatment may be an effective adjuvant for radiation therapy. Radiosensitizer drugs are highly sought after in the clinic, and a radiosensitizer lncRNA may be an effective substitute. To our knowledge, Lnc-RAINY is the first example of a therapeutic lncRNA that can be used to induce radiation sensitization.

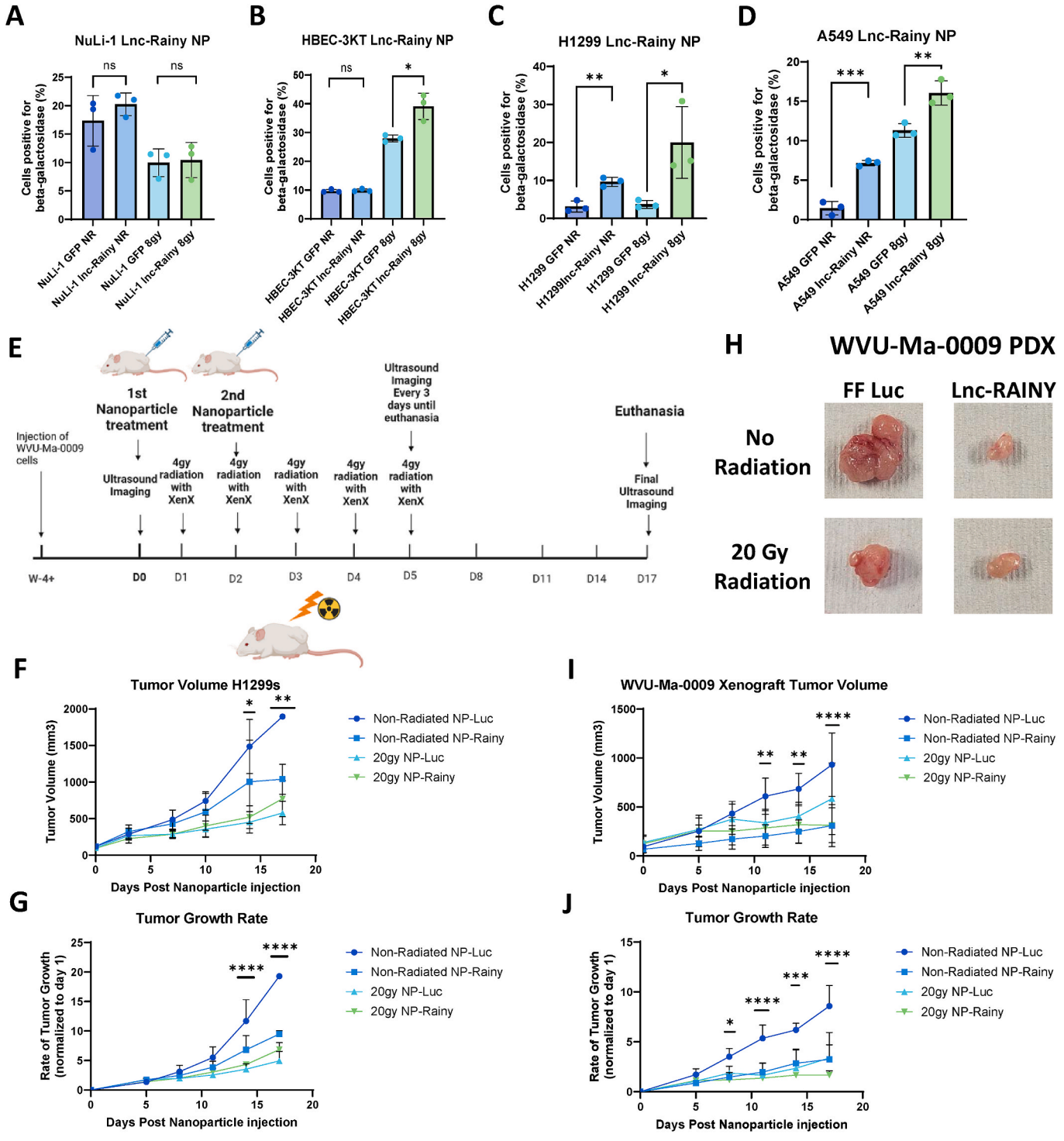

Fig. 6. lnc-RAINY can be delivered via nanoparticles to delay tumor growth.
A-B. Quantification of a Beta-galactosidase staining of NuLi-1 (A) and HBEC-3KT cells (B) with (8gy) and without (NR) radiation, having received lnc-RAINY or GFP mRNA loaded nanoparticles. **C-D.** Quantification of Beta-galactosidase staining of H1299 (C) and A549 cells (D) with and without radiation, having received lnc-RAINY or GFP mRNA loaded nanoparticles showing an increase in senescent cells after lnc-RAINY treatment. **E.** Schematic of tumor model performed on H1299 Xenograft and WVU-Ma-0009 PDX, created with BioRender.com. **F-G.** Tumor volume (F) and tumor growth rate (G) of H1299 Xenografts. **H.** Representative WVU-Ma-0009 tumors after treatment of lnc-RAINY or FF-luciferase mRNA loaded nanoparticles, with or without radiation treatment. **I-J.** Tumor volume (I) and tumor growth rate (J) of WVU-Ma-0009 PDX. Statistical analysis used was two-way ANOVA with Tukey's multiple comparison. Significance designation is against non-radiated Luciferase vs non-radiated lnc-RAINY. Error Bars (F–J): SD from the mean (n = 3 mice per group).

4. Discussion

Through these experiments, we have shown that lnc-RAINY is a lncRNA involved in radiation sensitization in NSCLC cells that regulates the transcription of specific genes important in cell cycle regulation, migration, and senescence. Primarily, lnc-RAINY interacts directly with the DNA in a triple helix R-loop to modify chromatin accessibility in specific promoter regions and cause changes in gene expression of important genes involved in radiation susceptibility such as CDC6 and CDC25A.

DNA:DNA:RNA triple helices, especially in R-loops, are crucial for regulating chromatin structure and have been known to impact gene expression. However, they are both known for causing and repairing DNA damage by using the RNA as a template [38]. Our data have shown the ability of lnc-RAINY to interact with the chromatin in these R-loops, likely acting as an intermediate, recognizing DNA damage, and preventing significant gene expression changes. It is possible that the interaction between lnc-RAINY and the chromatin is a preventative measure, allowing the cell to accumulate DNA damage and potentiate cell death, rather than allowing DNA repair mechanisms to persist and fix the damage.

There has been significant research into the effects of senescence on tumor cells, particularly after radiation treatment, as DNA damage is a major inducer of senescence. Senescence is stable cell cycle arrest; however, some cells are eventually able to evade this arrest and become aggressive again, whether by genetic changes or external pressure [39]. With the data presented here, particularly Fig. 6, it is possible that by increasing senescence, lnc-RAINY is decreasing the tumor burden, and limiting the number of cells that escape senescence due to external pressure.

Radiation has been shown to increase the frequency and aggressiveness of migration patterns of tumor cells after treatment [40]. Interestingly, lnc-RAINY decreased the migratory ability of cells after radiation. Further studies are necessary to test the metastatic capabilities of tumors after lnc-RAINY treatment *in vivo*, however, *in vitro* studies would suggest lnc-RAINY decreases the ability of cells to disseminate.

The cell cycle is critical for sensitivity to radiation therapy, with the stage impacting the pathways the cells use to signal and repair DNA damage [37,41]. CDC6 is a vital component of the replication complex in eukaryotes [42]. It is generally located within the nucleus in G1 phase but is translocated to the cytoplasm at the start of S phase [43]. CDC6 is an ATPase integral for loading the helicase onto DNA [44]. Further, its overexpression has been shown to decrease chromosome stability in NSCLC [45]. CDC25A has been shown to undergo degradation in response to DNA Damage [46]. Decreased expression of CDC25A has been shown to increase senescence in mammary epithelial cells [26]. Through interactions with both of these genes promoter regions, it is likely that lnc-RAINY is acting as a post-stress sensor, either helping or hindering the ability of cells to progress based on the severity of the damage.

This same phenomenon can be seen *in vivo* in both H1299 Xenograft and PDX models. Both the tumor volume and growth rate of the tumors that received lnc-RAINY were decreased. This trend was unexpected with regard to the non-radiated tumors. Without the DNA damage caused by the radiation, it was expected that tumors treated with lnc-RAINY nanoparticles would not grow as much as tumors treated with luciferase nanoparticles. However, what was observed was almost a complete regression to post radiation levels of growth, especially within the PDX model. Further studies are necessary to fully characterize the impact of lnc-RAINY *in vivo*, however, it can be suggested that just the presence of lnc-RAINY is enough to cause a shift in the growth patterns, leading to a slower growth rate and a decreased overall tumor burden.

Overall, these data show the mechanism behind the ability of lnc-RAINY to convey radiation sensitivity. Lnc-RAINY causes the differential expression of genes through modulation of chromatin opening via triple helix interactions with DNA. These interactions modulate the expression of critical cell cycle progression genes such as CDC6 and CDC25A. Interestingly, not only does this place stress on the cells to block their movement through the cell cycle, but it also impacts their migratory ability, and increases the number of cells converting to senescence (Fig. 7).

This study is limited by its usage of subcutaneous tumor placement. NSCLC, being tumors of the lung, requires testing of tumors in an orthotopic animal model. Further research needs to be done to adapt and scale the delivery of this treatment to increase tumor specificity, modify lipid nanoparticle composition, and improve the route of administration. For example, the used of mannosylated lipid nanoparticles have a higher affinity to target lung cancer cells enhancing drug delivery [47]. Furthermore, aerosolizable lipid nanoparticles can be develop to deliver RNA to the lungs opening the possibility to target NSCLC directly in the pulmonary region [48]. Nevertheless, we believe the results shown here are promising, and warrant further investigation into an orthotopic NSCLC animal model [49].

Interestingly, our data suggest that lnc-RAINY is most effective in a PDX environment, where the tumors are varied in their composition. Within the PDX data, lnc-RAINY treatment was as effective as radiation treatment, and the two treatments showed a minor synergistic effect. The data presented here suggest lnc-RAINY may be given as a treatment in place of radiation therapy, particularly in patients where radiation may not be a viable option. Further, while most male NSCLC tumors do not have a complete loss of Y chromosome, many cells within the tumor microenvironment retain their Y chromosome. These data suggest that lnc-RAINY may interact with the cells in the tumor microenvironment to increase the tumor's susceptibility to DNA damage. It is important to acknowledge the clinical impact of male versus female as well. Further investigation is required to understand lnc-RAINY's impact on female tumors, but for male patients, lnc-RAINY nanoparticle treatment offers a radio sensitization effect across the tumor, while minimizing impact to surrounding tissues.

To our knowledge, this is the first example of a lncRNA that increases radiation sensitivity through direct interactions with DNA. Significant research in lncRNA functions have identified many competitive endogenous lncRNAs, such as TPTEP1 [50], which may sponge microRNAs, impacting well known radiation resistance pathways, or lncRNAs that interact with proteins to impact radiation response pathways such as linc00312 or lncRNA-NKILA [51,52]. To date, many reviews have uncovered the vast volume of research that pertains to lncRNAs and their roles in mediating or exacerbating radiation resistance, such as those posed by Podralska et al. Wu et al., and Zhang et al. [53–55]. However, there has been little evidence to show a lncRNA that directly interacts with the DNA and can increase radiation sensitivity.

Important limitations to this study include the need to further characterize the impact of lnc-RAINY on female cells and tumors. Because the Y chromosome is specific to the male population, lnc-RAINY does not exist in females. Therefore, there is a need to understand the impact of lnc-RAINY when delivered via nanoparticles to female tumors and patient derived xenografts. Further, the Y chromosome is lost in many cancers, leading to a mosaic of Y chromosome positive and negative cells within the tumors, and the impact of the percentage of Y chromosome positive cells on lnc-RAINY's function is unknown. Lnc-RAINY had a stronger effect on the PDX than the singular cell line H1299. Further studies will be necessary to characterize the impact of Y chromosome expressing cells on lnc-RAINY's viability as a treatment. Additionally, the PDXs utilized were injected subcutaneously, and treated with intra-tumoral injections. To truly identify the feasibility of nanoparticle loaded lnc-RAINY as a novel treatment modality, it needs to be delivered to orthotopic tumors.

Further studies are necessary to understand the potential of lnc-RAINY as a radio-sensitizing agent in other types of cancers such as prostate, head and neck, and colon cancers. Interestingly, while there are many radio-sensitizers that impact NSCLC *in vitro*, including some

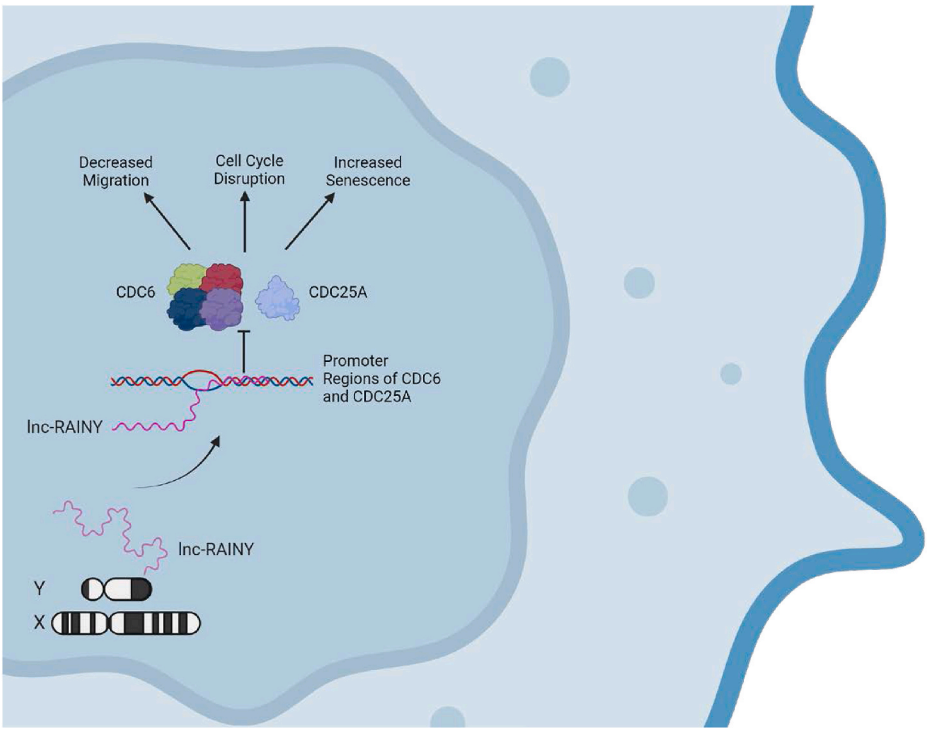

Fig. 7. Lnc-RAINY originates from the Y chromosome and acts through triple helix interactions to influence cell cycle progression, senescence and migration. Image created with Biorender.

small molecule inhibitors and chemotherapy agents[56–58], microRNAs, and siRNAs [59,60], there has been no further work investigating a multifunctional lncRNA as a radiosensitizer.

CRediT authorship contribution statement

Emily S. Westemeier-Rice: Writing – review & editing, Writing – original draft, Visualization, Validation, Project administration, Methodology, Investigation, Formal analysis, Data curation, Conceptualization. **Michael T. Winters:** Writing – review & editing, Validation, Methodology, Data curation. **Travis W. Rawson:** Writing – review & editing, Methodology, Data curation. **Kiran J. Patel:** Methodology, Data curation. **Olivia McHugh:** Methodology, Data curation. **Sierra Ward:** Methodology, Data curation. **Sarah McLaughlin:** Supervision, Methodology, Formal analysis, Data curation. **Amanda Stewart:** Writing – review & editing, Supervision, Data curation. **Bishal Misra:** Data curation. **Sebastian Dziadowicz:** Methodology, Data curation. **Weijun Yi:** Formal analysis. **Sharan Bobbala:** Methodology, Investigation. **Gangqing Hu:** Formal analysis. **Ivan Martinez:** Writing – review & editing, Visualization, Supervision, Resources, Methodology, Investigation, Funding acquisition, Formal analysis, Data curation, Conceptualization.

Data availability statement

The data generated in this study are publicly available in Gene Expression Omnibus (GEO) at GSE274484 and GSE274485.

Funding support

Emily Westemeier-Rice was supported by West Virginia University's Systems Toxicology T32 Training Grant, ES032920 from the United States National Institute of Health. Ivan Martinez, Ph.D. was supported by a Research Scholar Grants, RSG-24-1039619-01-RMC, Grant DOI #: 1039619, from the American Cancer Society.

Declaration of competing interest

The authors declare no conflicts of interest.

Acknowledgements

We thank the West Virginia University Animal Models & Imaging Facility and their funding sources (NIH grants P20RR016440, P30GM103488, S10RR026378, U54GM104942, P20GM103434) for their assistance with cell imaging, the irradiator and instrument training. We would also like to thank Dr. Kathy Brundage and the WVU Flow Cytometry and Single Cell Core Facility (RRID: SCR_017738, LSR Fortessa: S10 Equipment grant #OD016165) for their support with the LSR Fortessa training. We would further like to thank the Bioinformatics Core Facility at WVU for their support with bulk RNA and ATAC-Seq analysis.

Appendix A. Supplementary data

Supplementary data to this article can be found online at https://doi.org/10.1016/j.ncrna.2024.12.004.

References

[1] F Bray, M Laversanne, H Sung, J Ferlay, RL Siegel, I Soerjomataram, A. Jemal, Global cancer statistics 2022: GLOBOCAN estimates of incidence and mortality worldwide for 36 cancers in 185 countries, CA Cancer J. Clin. 74 (3) (2024) 229–263, https://doi.org/10.3322/caac.21834. Epub 2024 Apr 4. PMID: 38572751.

[2] National Cancer Institute, SEER*Explorer Application, Surveillance, Epidemiology and End Results Program (n.d.). https://seer.cancer.gov/statistics-network/explorer/application.html?site=47&data_type=2&graph_type=10&compareBy=sex&chk_sex_3=3&chk_sex_2=2&series=9&race=1&age_range=1&advopt_precision=1&advopt_show_ci=on&hdn_view=0#resultsRegion0 (accessed October 22, 2023).

[3] R.L. Siegel, K.D. Miller, N.S. Wagle, A. Jemal, Cancer statistics, CA A Cancer J. Clin. 73 (2023) 17–48, https://doi.org/10.3322/caac.21763, 2023.

[4] J. Theys, S. Yahyanejad, R. Habets, P. Span, L. Dubois, K. Paesmans, B. Kattenbeld, J. Cleutjens, A.J. Groot, O.C.J. Schuurbiers, P. Lambin, J. Bussink, M. Vooijs, High

NOTCH activity induces radiation resistance in non small cell lung cancer, Radiother. Oncol. 108 (2013) 440–445, https://doi.org/10.1016/j.radonc.2013.06.020.
[5] O.C.J. Schuurbiers, J.H.A.M. Kaanders, H.F.M. van der Heijden, R.P.N. Dekhuijzen, W.J.G. Oyen, J. Bussink, The PI3-K/AKT-Pathway and radiation resistance mechanisms in non-small cell lung cancer, J. Thorac. Oncol. 4 (2009) 761–767, https://doi.org/10.1097/JTO.0b013e3181a1084f.
[6] H. Yin, X. Wang, X. Zhang, Y. Zeng, Q. Xu, W. Wang, F. Zhou, Y. Zhou, UBE2T promotes radiation resistance in non-small cell lung cancer via inducing epithelial-mesenchymal transition and the ubiquitination-mediated FOXO1 degradation, Cancer Lett. 494 (2020) 121–131, https://doi.org/10.1016/j.canlet.2020.06.005.
[7] K. Gurtner, Z. Kryzmien, L. Koi, M. Wang, C.H. Benes, S. Hering, H. Willers, M. Baumann, M. Krause, Radioresistance of KRAS/TP53-mutated lung cancer can be overcome by radiation dose escalation or EGFR tyrosine kinase inhibition in vivo, Int. J. Cancer 147 (2020) 472–477, https://doi.org/10.1002/ijc.32598.
[8] C. Richard Boland, Non-coding RNA: it's not junk, Dig. Dis. Sci. 62 (2017) 1107–1109, https://doi.org/10.1007/s10620-017-4506-1.
[9] Y. Luo, B.C. Hitz, I. Gabdank, J.A. Hilton, M.S. Kagda, B. Lam, Z. Myers, P. Sud, J. Jou, K. Lin, U.K. Baymuradov, K. Graham, C. Litton, S.R. Miyasato, J.S. Strattan, O. Jolanki, J.-W. Lee, F.Y. Tanaka, P. Adenekan, E. O'Neill, J.M. Cherry, New developments on the Encyclopedia of DNA Elements (ENCODE) data portal, Nucleic Acids Res. 48 (2020) D882–D889, https://doi.org/10.1093/nar/gkz1062.
[10] L. Zhao, J. Wang, Y. Li, T. Song, Y. Wu, S. Fang, D. Bu, H. Li, L. Sun, D. Pei, Y. Zheng, J. Huang, M. Xu, R. Chen, Y. Zhao, S. He, NONCODEV6: an updated database dedicated to long non-coding RNA annotation in both animals and plants, Nucleic Acids Res. 49 (2021) D165–D171, https://doi.org/10.1093/nar/gkaa1046.
[11] A. Dong, C.B. Preusch, W.-K. So, K. Lin, S. Luan, R. Yi, J.W. Wong, Z. Wu, T. H. Cheung, A long noncoding RNA, LncMyoD, modulates chromatin accessibility to regulate muscle stem cell myogenic lineage progression, Proc. Natl. Acad. Sci. USA 117 (2020) 32464–32475, https://doi.org/10.1073/pnas.2005868117.
[12] I. Pavlaki, F. Alammari, B. Sun, N. Clark, T. Sirey, S. Lee, D.J. Woodcock, C. P. Ponting, F.G. Szele, K.W. Vance, The long non-coding RNA Paupar promotes KAP1-dependent chromatin changes and regulates olfactory bulb neurogenesis, EMBO J. 37 (2018) e98219, https://doi.org/10.15252/embj.201798219.
[13] X. Zhang, Y. Zhou, S. Chen, W. Li, W. Chen, W. Gu, LncRNA MACC1-AS1 sponges multiple miRNAs and RNA-binding protein PTBP1, Oncogenesis 8 (2019) 1–13, https://doi.org/10.1038/s41389-019-0182-7.
[14] W. Tian, Y. Du, Y. Ma, L. Gu, J. Zhou, D. Deng, MALAT1–miR663a negative feedback loop in colon cancer cell functions through direct miRNA–lncRNA binding, Cell Death Dis. 9 (2018) 1–12, https://doi.org/10.1038/s41419-018-0925-y.
[15] Z. Xing, Y. Zhang, K. Liang, L. Yan, Y. Xiang, C. Li, Q. Hu, F. Jin, V. Putluri, N. Putluri, C. Coarfa, A. Sreekumar, P.K. Park, T.K. Nguyen, S. Wang, J. Zhou, Y. Zhou, J.R. Marks, D.H. Hawke, M.-C. Hung, L. Yang, L. Han, H. Ying, C. Lin, Expression of long noncoding RNA YIYA promotes glycolysis in breast cancer, Cancer Res. 78 (2018) 4524–4532, https://doi.org/10.1158/0008-5472.CAN-17-0385.
[16] C. Liu, Z. Peng, P. Li, H. Fu, J. Feng, Y. Zhang, T. Liu, Y. Liu, Q. Liu, Q. Liu, D. Li, M. Wu, lncRNA RMST suppressed GBM cell mitophagy through enhancing FUS SUMOylation, Mol. Ther. Nucleic Acids 19 (2020) 1198–1208, https://doi.org/10.1016/j.omtn.2020.01.008.
[17] T. Brownmiller, J.A. Juric, A.D. Ivey, B.M. Harvey, E.S. Westemeier, M.T. Winters, A.M. Stevens, A.N. Stanley, K.E. Hayes, S.A. Sprowls, A.S.G. Ammer, M. Walker, E. A. Bey, X. Wu, Z.-F. Lim, L. Zhu, S. Wen, G. Hu, P.C. Ma, I. Martinez, Y chromosome LncRNA are involved in radiation response of male non-small cell lung cancer cells, Cancer Res. 80 (2020) 4046–4057, https://doi.org/10.1158/0008-5472.CAN-19-4032.
[18] S. Jayaseelan, F. Doyle, S. Currenti, S.A. Tenenbaum, RIP: an mRNA localization Technique, in: J.E. Gerst (Ed.), RNA Detection and Visualization: Methods and Protocols, Humana Press, Totowa, NJ, 2011, pp. 407–422, https://doi.org/10.1007/978-1-61779-005-8_25.
[19] H.R. Gibbons, T.M. Aune, Immunoprecipitation of DNA:RNA hybrids using the S9.6 antibody, Methods Mol. Biol. 2161 (2020) 195–207, https://doi.org/10.1007/978-1-0716-0680-3_14.
[20] B. Misra, K.A. Hughes, W.H. Pentz, P. Samart, W.J. Geldenhuys, S. Bobbala, Flash nanoprecipitation assisted self-assembly of ionizable lipid nanoparticles for nucleic acid delivery, Nanoscale 16 (2024) 6939–6948, https://doi.org/10.1039/D4NR00278D.
[21] A. Rhie, S. Nurk, M. Cechova, S.J. Hoyt, D.J. Taylor, N. Altemose, P.W. Hook, S. Koren, M. Rautiainen, I.A. Alexandrov, J. Allen, M. Asri, A.V. Bzikadze, N.-C. Chen, C.-S. Chin, M. Diekhans, P. Flicek, G. Formenti, A. Fungtammasan, C. Garcia Giron, E. Garrison, A. Gershman, J.L. Gerton, P.G.S. Grady, A. Guarracino, L. Haggerty, R. Halabian, N.F. Hansen, R. Harris, G.A. Hartley, W. T. Harvey, M. Haukness, J. Heinz, T. Hourlier, R.M. Hubley, S.E. Hunt, S. Hwang, M. Jain, R.K. Kesharwani, A.P. Lewis, H. Li, G.A. Logsdon, J.K. Lucas, W. Makalowski, C. Markovic, F.J. Martin, A.M. Mc Cartney, R.C. McCoy, J. McDaniel, B.M. McNulty, P. Medvedev, A. Mikheenko, K.M. Munson, T. D. Murphy, H.E. Olsen, N.D. Olson, L.F. Paulin, D. Porubsky, T. Potapova, F. Ryabov, S.L. Salzberg, M.E.G. Sauria, F.J. Sedlazeck, K. Shafin, V.A. Shepelev, A. Shumate, J.M. Storer, L. Surapaneni, A.M. Taravella Oill, F. Thibaud-Nissen, W. Timp, M. Tomaszkiewicz, M.R. Vollger, B.P. Walenz, A.C. Watwood, M. H. Weissensteiner, A.M. Wenger, M.A. Wilson, S. Zarate, Y. Zhu, J.M. Zook, E. E. Eichler, R.J. O'Neill, M.C. Schatz, K.H. Miga, K.D. Makova, A.M. Phillippy, The complete sequence of a human Y chromosome, Nature 621 (2023) 344–354, https://doi.org/10.1038/s41586-023-06457-y.
[22] P.-J. Volders, J. Anckaert, K. Verheggen, J. Nuytens, L. Martens, P. Mestdagh, J. Vandesompele, LNCipedia 5: towards a reference set of human long non-coding RNAs, Nucleic Acids Res. 47 (2019) D135–D139, https://doi.org/10.1093/nar/gky1031.
[23] Z. Jehan, S. Vallinayagam, S. Tiwari, S. Pradhan, L. Singh, A. Suresh, H.M. Reddy, Y.R. Ahuja, R.A. Jesudasan, Novel noncoding RNA from human Y distal heterochromatic block (Yq12) generates testis-specific chimeric CDC2L2, Genome Res. 17 (2007) 433–440, https://doi.org/10.1101/gr.5155706.
[24] S. Chen, X. Chen, G. Xie, Y. He, D. Yan, D. Zheng, S. Li, X. Fu, Y. Li, X. Pang, Z. Hu, H. Li, W. Tan, J. Li, Cdc6 contributes to cisplatin-resistance by activation of ATR-Chk1 pathway in bladder cancer cells, Oncotarget 7 (2016) 40362–40376, https://doi.org/10.18632/oncotarget.9616.
[25] F. Wang, F. Zhao, L. Zhang, L. Xiong, Q. Mao, Y. Liu, X. Qiu, X. Wang, L. Shui, X. Chen, K. Ren, P. Shui, Q. Zhang, Y. Deng, W. Li, X. Xie, D. Wu, T. Li, J. Lang, L. Liu, H. Chen, J. Xu, S. Bai, Z. Li, Q. Yue, N. Chen, B. Zhou, C. Yi, Y. Wei, Y. Fu, Y. Luo, Q. Gou, L. Liu, Y. Liu, J. Kang, J. Wang, D. Jing, F. Zhang, X. Yang, X. Li, T. Jiang, Z. Zhang, Y. Zhou, J. Yi, CDC6 is a prognostic biomarker and correlated with immune infiltrates in glioma, Mol. Cancer 21 (2022) 153, https://doi.org/10.1186/s12943-022-01623-8.
[26] C. Sandhu, J. Donovan, N. Bhattacharya, M. Stampfer, P. Worland, J. Slingerland, Reduction of Cdc25A contributes to cyclin E1-Cdk2 inhibition at senescence in human mammary epithelial cells, Oncogene 19 (2000) 5314–5323, https://doi.org/10.1038/sj.onc.1203908.
[27] R.A. Avelar, J.G. Ortega, R. Tacutu, E.J. Tyler, D. Bennett, P. Binetti, A. Budovsky, K. Chatsirisupachai, E. Johnson, A. Murray, S. Shields, D. Tejada-Martinez, D. Thornton, V.E. Fraifeld, C.L. Bishop, J.P. de Magalhães, A multidimensional systems biology analysis of cellular senescence in aging and disease, Genome Biol. 21 (2020) 91, https://doi.org/10.1186/s13059-020-01990-9.
[28] M. Zhang, J. Wu, W. Zhong, Z. Zhao, W. He, DNA-methylation-induced silencing of DIO3OS drives non-small cell lung cancer progression via activating hnRNPK-MYC-CDC25A axis, Molecular Therapy - Oncolytics 23 (2021) 205–219, https://doi.org/10.1016/j.omto.2021.09.006.
[29] N.H. Patel, S.S. Sohal, M.H. Manjili, J.C. Harrell, D.A. Gewirtz, The roles of autophagy and senescence in the tumor cell response to radiation, Radiat. Res. 194 (2020) 103–115, https://doi.org/10.1667/RADE-20-00009.
[30] M. Vilalta, M. Rafat, E.E. Graves, Effects of radiation on metastasis and tumor cell migration, Cell. Mol. Life Sci. 73 (2016) 2999–3007, https://doi.org/10.1007/s00018-016-2210-5.
[31] U.K. Muppirala, V.G. Honavar, D. Dobbs, Predicting RNA-protein interactions using only sequence information, BMC Bioinf. 12 (2011) 489, https://doi.org/10.1186/1471-2105-12-489.
[32] S. Cohen, N. Puget, Y.-L. Lin, T. Clouaire, M. Aguirrebengoa, V. Rocher, P. Pasero, Y. Canitrot, G. Legube, Senataxin resolves RNA:DNA hybrids forming at DNA double-strand breaks to prevent translocations, Nat. Commun. 9 (2018) 533, https://doi.org/10.1038/s41467-018-02894-w.
[33] E. Tumini, S. Barroso, C.P. Calero, A. Aguilera, Roles of human POLD1 and POLD3 in genome stability, Sci. Rep. 6 (2016) 38873, https://doi.org/10.1038/srep38873.
[34] M.S. Leisegang, J.K. Bains, S. Seredinski, J.A. Oo, N.M. Krause, C.-C. Kuo, S. Günther, N. Sentürk Cetin, T. Warwick, C. Cao, F. Boos, J. Izquierdo Ponce, S. Haydar, R. Bednarz, C. Valasarajan, D.C. Fuhrmann, J. Preussner, M. Looso, S. S. Pullamsetti, M.H. Schulz, H.R.A. Jonker, C. Richter, F. Rezende, R. Gilsbach, B. Pflüger-Müller, I. Wittig, I. Grummt, T. Ribarska, I.G. Costa, H. Schwalbe, R. P. Brandes, HIF1α-AS1 is a DNA:DNA:RNA triplex-forming lncRNA interacting with the HUSH complex, Nat. Commun. 13 (2022) 6563, https://doi.org/10.1038/s41467-022-34252-2.
[35] C.-C. Kuo, S. Hänzelmann, N. Sentürk Cetin, S. Frank, B. Zajzon, J.-P. Derks, V. S. Akhade, G. Ahuja, C. Kanduri, I. Grummt, L. Kurian, I.G. Costa, Detection of RNA–DNA binding sites in long noncoding RNAs, Nucleic Acids Res. 47 (2019) e32, https://doi.org/10.1093/nar/gkz037.
[36] M. Césaire, J. Montanari, H. Curcio, D. Lerouge, R. Gervais, P. Demontrond, J. Balosso, F. Chevalier, Radioresistance of non-small cell lung cancers and therapeutic perspectives, Cancers 14 (2022) 2829, https://doi.org/10.3390/cancers14122829.
[37] T.M. Pawlik, K. Keyomarsi, Role of cell cycle in mediating sensitivity to radiotherapy, Int. J. Radiat. Oncol. Biol. Phys. 59 (2004) 928–942, https://doi.org/10.1016/j.ijrobp.2004.03.005.
[38] E. Petermann, L. Lan, L. Zou, Sources, resolution and physiological relevance of R-loops and RNA–DNA hybrids, Nat. Rev. Mol. Cell Biol. 23 (2022) 521–540, https://doi.org/10.1038/s41580-022-00474-x.
[39] C.A. Schmitt, B. Wang, M. Demaria, Senescence and cancer — role and therapeutic opportunities, Nat. Rev. Clin. Oncol. 19 (2022) 619–636, https://doi.org/10.1038/s41571-022-00668-4.
[40] M. Merrick, M.J. Mimlitz, C. Weeder, H. Akhter, A. Bray, A. Walther, C. Nwakama, J. Bamesberger, H. Djam, K. Abid, A. Ekpenyong, In vitro radiotherapy and chemotherapy alter migration of brain cancer cells before cell death, Biochemistry and Biophysics Reports 27 (2021) 101071, https://doi.org/10.1016/j.bbrep.2021.101071.
[41] F.J. Groelly, M. Fawkes, R.A. Dagg, A.N. Blackford, M. Tarsounas, Targeting DNA damage response pathways in cancer, Nat. Rev. Cancer 23 (2023) 78–94, https://doi.org/10.1038/s41568-022-00535-5.
[42] L.R. Borlado, J. Méndez, CDC6: from DNA replication to cell cycle checkpoints and oncogenesis, Carcinogenesis 29 (2008) 237–243, https://doi.org/10.1093/carcin/bgm268.
[43] S. Ohta, M. Koide, T. Tokuyama, N. Yokota, S. Nishizawa, H. Namba, Cdc6 expression as a marker of proliferative activity in brain tumors, Oncol. Rep. 8 (2001) 1063–1066, https://doi.org/10.3892/or.8.5.1063.

[44] M. Pinyol, I. Salaverria, S. Bea, V. Fernández, L. Colomo, E. Campo, P. Jares, Unbalanced expression of licensing DNA replication factors occurs in a subset of mantle cell lymphomas with genomic instability, Int. J. Cancer 119 (2006) 2768–2774, https://doi.org/10.1002/ijc.22146.
[45] P. Karakaidos, S. Taraviras, L.V. Vassiliou, P. Zacharatos, N.G. Kastrinakis, D. Kougiou, M. Kouloukoussa, H. Nishitani, A.G. Papavassiliou, Z. Lygerou, V. G. Gorgoulis, Overexpression of the replication licensing regulators hCdt1 and hCdc6 characterizes a subset of non-small-cell lung carcinomas: synergistic effect with mutant p53 on tumor growth and chromosomal instability—evidence of E2F-1 transcriptional control over hCdt1, Am. J. Pathol. 165 (2004) 1351–1365, https://doi.org/10.1016/S0002-9440(10)63393-7.
[46] Tao Shen, Shile Huang, The role of Cdc25A in the regulation of cell proliferation and apoptosis, Anti Cancer Agents Med. Chem. 12 (2012) 631–639, https://doi.org/10.2174/187152012800617678.
[47] N. Soni, N. Soni, H. Pandey, R. Maheshwari, P. Kesharwani, R.K. Tekade, Augmented delivery of gemcitabine in lung cancer cells exploring mannose anchored solid lipid nanoparticles, J. Colloid Interface Sci. 481 (2016) 107–116, https://doi.org/10.1016/j.jcis.2016.07.020.
[48] H. Zhang, J. Leal, M.R. Soto, H.D.C. Smyth, D. Ghosh, Aerosolizable lipid nanoparticles for pulmonary delivery of mRNA through design of experiments, Pharmaceutics 12 (2020) 1042, https://doi.org/10.3390/pharmaceutics12111042.
[49] A.K. Patel, J.C. Kaczmarek, S. Bose, K.J. Kauffman, F. Mir, M.W. Heartlein, F. DeRosa, R. Langer, D.G. Anderson, Inhaled nanoformulated mRNA polyplexes for protein production in lung epithelium, Adv. Mater. 31 (2019) 1805116, https://doi.org/10.1002/adma.201805116.
[50] T. Tang, L.-X. Wang, M.-L. Yang, R.-M. Zhang, lncRNA TPTEP1 inhibits stemness and radioresistance of glioma through miR-106a-5p-mediated P38 MAPK signaling, Mol. Med. Rep. 22 (2020) 4857–4867, https://doi.org/10.3892/mmr.2020.11542.
[51] Z. Guo, Y.-H. Wang, H. Xu, C.-S. Yuan, H.-H. Zhou, W.-H. Huang, H. Wang, W. Zhang, LncRNA linc00312 suppresses radiotherapy resistance by targeting DNA-PKcs and impairing DNA damage repair in nasopharyngeal carcinoma, Cell Death Dis. 12 (2021) 69, https://doi.org/10.1038/s41419-020-03302-2.
[52] T. Yang, S. Li, J. Liu, D. Yin, X. Yang, Q. Tang, lncRNA-NKILA/NF-κB feedback loop modulates laryngeal cancer cell proliferation, invasion, and radioresistance, Cancer Med. 7 (2018) 2048–2063, https://doi.org/10.1002/cam4.1405.
[53] M. Podralska, S. Ciesielska, J. Kluiver, A. van den Berg, A. Dzikiewicz-Krawczyk, I. Slezak-Prochazka, Non-coding RNAs in cancer radiosensitivity: MicroRNAs and lncRNAs as regulators of radiation-induced signaling pathways, Cancers 12 (2020) 1662, https://doi.org/10.3390/cancers12061662.
[54] H. Zhang, C. Fang, Z. Feng, T. Xia, L. Lu, M. Luo, Y. Chen, Y. Liu, Y. Li, The role of LncRNAs in the regulation of radiotherapy sensitivity in cervical cancer, Front. Oncol. 12 (2022) 896840, https://doi.org/10.3389/fonc.2022.896840.
[55] W. Wu, S. Zhang, J. He, The mechanism of long non-coding RNA in cancer radioresistance/radiosensitivity: a systematic review, Front. Pharmacol. 13 (2022), https://doi.org/10.3389/fphar.2022.879704.
[56] S.G.J.A. Peeters, C.M.L. Zegers, R. Biemans, N.G. Lieuwes, R.G.P.M. van Stiphout, A. Yaromina, J.D. Sun, C.P. Hart, A.D. Windhorst, W. van Elmpt, L.J. Dubois, P. Lambin, TH-302 in combination with radiotherapy enhances the therapeutic outcome and is associated with pretreatment [18F]HX4 hypoxia PET imaging, Clin. Cancer Res. 21 (2015) 2984–2992, https://doi.org/10.1158/1078-0432.CCR-15-0018.
[57] N. Kubo, S. Noda, A. Takahashi, Y. Yoshida, T. Oike, K. Murata, A. Musha, Y. Suzuki, T. Ohno, T. Takahashi, T. Nakano, Radiosensitizing effect of carboplatin and paclitaxel to carbon-ion beam irradiation in the non-small-cell lung cancer cell line H460, J. Radiat. Res. 56 (2015) 229–238, https://doi.org/10.1093/jrr/rru085.
[58] Y. Zhao, L. Wang, Q. Huang, Y. Jiang, J. Wang, L. Zhang, Y. Tian, H. Yang, Radiosensitization of non-small cell lung cancer cells by inhibition of TGF-β1 signaling with SB431542 is dependent on p53 status, Oncol. Res. 24 (2016) 1–7, https://doi.org/10.3727/096504016X14570992647087.
[59] H. Yin, J. Ma, L. Chen, S. Piao, Y. Zhang, S. Zhang, H. Ma, Y. Li, Y. Qu, X. Wang, Q. Xu, MiR-99a enhances the radiation sensitivity of non-small cell lung cancer by targeting mTOR, Cell. Physiol. Biochem. 46 (2018) 471–481, https://doi.org/10.1159/000488615.
[60] L. Song, L. Peng, S. Hua, X. Li, L. Ma, J. Jie, D. Chen, Y. Wang, D. Li, miR-144-5p enhances the radiosensitivity of non-small-cell lung cancer cells via targeting ATF2, BioMed Res. Int. 2018 (2018) e5109497, https://doi.org/10.1155/2018/5109497.